Quarterly Reviews of Biophysics

cambridge.org/qrb

Macromolecular room temperature crystallography

Marcus Fischer[1,2]

[1]Department of Chemical Biology & Therapeutics, St. Jude Children's Research Hospital, Memphis, TN 38105, USA and [2]Department of Structural Biology, St. Jude Children's Research Hospital, Memphis, TN 38105, USA

Review

Cite this article: Fischer M (2021). Macromolecular room temperature crystallography. *Quarterly Reviews of Biophysics* **54**, e1, 1–15. https://doi.org/10.1017/S0033583520000128

Received: 8 June 2020
Revised: 23 October 2020
Accepted: 1 December 2020

Key words:
Cryogenic trapping; energy landscape; room temperature; structural dynamics; variable temperature; X-ray crystallography

Author for correspondence:
Marcus Fischer,
E-mail: marcus.fischer@stjude.org

Abstract

X-ray crystallography enables detailed structural studies of proteins to understand and modulate their function. Conducting crystallographic experiments at cryogenic temperatures has practical benefits but potentially limits the identification of functionally important alternative protein conformations that can be revealed only at room temperature (RT). This review discusses practical aspects of preparing, acquiring, and analyzing X-ray crystallography data at RT to demystify preconceived impracticalities that freeze progress of routine RT data collection at synchrotron sources. Examples are presented as conceptual and experimental templates to enable the design of RT-inspired studies; they illustrate the diversity and utility of gaining novel insights into protein conformational landscapes. An integrative view of protein conformational dynamics enables opportunities to advance basic and biomedical research.

Table of contents

Introduction

The introduction of cryogenic X-ray crystallography into structural biology led to an explosion of protein structural information (Garman and Schneider, 1997; Garman, 1999; Burley *et al.*, 2018). Its practical benefits are convincing: long-term storage, easy handling, and transport of crystals in dry shipping containers that enable remote data collection. Arguably, the most important benefit is that cryogenic temperatures mitigate radiation damage of the protein (Holton, 2009). This is achieved by reducing secondary radiation damage by decreasing diffusion rates of deleterious radicals and other damaging species (Garman, 1999; Juers and Matthews, 2004; Garman and Owen, 2006; Holton, 2009; Warkentin *et al.*, 2013; Garman and Weik, 2017). Analogously, flash-cooling has been used to trap catalytic intermediates (Makinen and Fink, 1977; Fink and Petsko, 1981; Moffat and Henderson, 1995; Weik and Colletier, 2010). In turn, this raises the question of whether protein residues important for function may also be trapped in nonphysiological conformations.

Approaches of cooling crystals to reduce radiation damage date back to the 1970s but were initially abandoned due to undesirable increases in mosaicity (Low *et al.*, 1966) before reasonable isomorphism was obtained for frozen crystals (Haas and Rossmann, 1970). To avoid

CAMBRIDGE UNIVERSITY PRESS

deleterious ice formation in protein channels, Petsko introduced the use of cryoprotective mother liquors (Petsko, 1975). This allowed several freeze/thaw cycles of the crystal but was deemed cumbersome, preventing its wide-spread use. At the time, the same fate awaited other pioneering approaches including rapid cooling of crystals in liquid propane (Hartmann *et al.*, 1982) and slow crystal cooling (Drew *et al.*, 1982), despite their promise of providing insights into conformational substates in metmyoglobin and the B-DNA dodecamer, respectively. In 1988, Håkon Hope introduced a general method of cryoprotecting protein crystals in oil for X-ray crystallography (Hope, 1988). The approach facilitates crystal handling and the collection of high-resolution datasets while reducing radiation damage (Henderson, 1990). One of its first successful applications was ribosomal crystallography (Hope *et al.*, 1989), which enabled key structural studies on fragile crystals of ribosomal subunits and led to the Nobel Prize in Chemistry in 2009. At the same time, developments of crystal looping methods facilitated crystal handling (Teng, 1990) and a variety of suitable materials were tested in the early 1990s. With the impracticalities of cryocrystallography resolved, the field embraced the method for its practical merits and has since produced an exponentially increasing amount of structural data deposited into the Protein Data Bank (PDB) (Burley *et al.*, 2018) (Fig. 1). Coincidentally, the percentage of datasets collected per year at room temperature (RT) has dropped steadily since Garman and Schneider's seminal paper on 'macromolecular cryocrystallography,' which was published more than 20 years ago (Garman and Schneider, 1997).

Pioneering work in multitemperature crystallography dates back to 1979, when Frauenfelder *et al.*, shifted temperature from 220 to 300 K to probe the spatial distribution of protein structural dynamics in metmyoglobin (Frauenfelder *et al.*, 1979). Tilton *et al.* later extended the temperature range from 98 to 320 K and found that crystallographic B-factors of RNase A show a temperature-dependent biphasic response (Tilton *et al.*, 1992). The investigators also noted a correlation with the dynamic structure of the surrounding protein solvent. Temperature-derivative fluorescence spectroscopy studies suggested that the dynamics of crystalline proteins strongly depend on the solvent composition and crystal channels (Weik *et al.*, 2004). Work by Juers and Matthews provided a rare example in which a single crystal was successfully re-cycled between RT and low temperature. They proposed that protein distortions due to cryocooling warrant caution (Juers and Matthews, 2001). This 'two-state' model is reminiscent of Halle's work (Halle, 2004) on the glass transition temperature (~200 K) (Ringe and Petsko, 2003) and kinetic trapping of the protein upon flash-cooling. Moving across the glass transition was later exploited to demonstrate *in crystallo* substrate turnover when a crystal was warmed to 220 K (Ding *et al.*, 2006). Since Fraser *et al.*, established a mechanistic link between protein function and protein conformational ensembles observed only at RT (Fraser *et al.*, 2009), several articles have reinforced the notion that functionally important conformations that are hidden at cryogenic temperatures can be revealed by shifting temperature (Keedy *et al.*, 2014; 2015*b*). RT crystallography at synchrotron sources has since been applied to studying ligand binding (Fischer *et al.*, 2015), ligand discovery (Fischer *et al.*, 2014), and characterizing functional contact networks (van den Bedem *et al.*, 2013).

However, of all PDB structures with explicit temperature records, under 6% were collected at RT, i.e. cryogenic datasets make up approximately 94% of PDB structures (Fig. 1). Over the past decade, the percentage of RT datasets has remained steadily below 5%. Notably, the range of resolutions obtained at RT follows a similar distribution to that at cryogenic temperatures. While the benefits of cryocooling are well appreciated, some of its downsides include the need to use and optimize cryoprotectants (Alcorn and Juers, 2010; Tyree *et al.*, 2018), crystal damage, ice rings that interfere with diffraction from the protein lattice (Thorn *et al.*, 2017), and exaggerated crystal disorder such as increased mosaicity and R_{merge} values (Ravelli and McSweeney, 2000; Pflugrath, 2015). However, the main problem of common cryocooling is that the protein vitrifies on the intermediate timescale – it is neither fast nor slow (Halle, 2004). This traps a mix of conformational states that is not necessarily representative of the physiologically relevant state at equilibrium. Note that even for the same experimenter and protein, varying levels of the cold liquid nitrogen (LN_2) gas layer above the glass or foam dewar, as well as varying crystal sizes lead to differences in the freezing rate of crystals.

This review aims to dispel myths about RT X-ray crystallography (RTX) data collection and to provide practical guidance to facilitate collecting more dynamic protein structural data above the glass transition temperature. Advice is aimed to assist experimenters at all stages: before, during, and after the collection of crystallographic data at RT. The review ends with a selection of RTX studies that exemplify ways to gain dynamic insights into protein structures. The examples represent the breadth, rather than depth, of the field to illustrate both the novelty and value of the method to inform basic and biomedical research.

Before: how to prepare for RTX data collection

Crystal transport

One practical benefit of cryogenic methods becomes immediately apparent when pre-grown crystals need to be transported to a synchrotron – we have to find an alternative to the convenience of sending stably frozen crystals in a cryogenic shipping container. A few popular choices for sizeable (macro) crystals include classic capillary mounting (King, 1954; Basavappa *et al.*, 2003) (Fig. 2*c*), using pins that hold pre-mounted crystals (Fig. 2*b*), or juggling crystals to the synchrotron in their crystallization tray. Note that pre-mounted crystals protected by a thin-walled polyester sleeve (MiTeGen) with stabilizing solution (Fig. 2*b*) should be sent via ground transit because pressure changes during a flight can have undesirable effects, including dislodging the sleeve that protects crystals from dehydration. To prevent splashing in crystal trays upfront, it is worth exploring if crystallization is transferable to an *in situ* crystallization tray format. As the name indicates, *in situ* plates allow the screening of crystals without removing them from the tray. The *In Situ*-1™ plate (MiTeGen) allows crystals to be grown, transported and collected directly in the plate. Given its construction, the *In Situ*-1™ plate promises optional long-distance shipping with reduced cross-contamination of fluid from reservoirs to the protein growth areas due to micro ledges that are absent in conventional plates (Fig. 2*d*). Alternatively, the Stanford Synchrotron Radiation Lightsource (SSRL) Crystallization Plate Kit (Crystal Positioning Systems; MiTeGen) allows *in situ* crystallization of proteins on substrates affixed to magnetic sample pin bases (Martiel *et al.*, 2019). This setup enables the transport of crystals mounted in loops, grids or capillaries in a controlled humidity environment to the synchrotron beamline for robotic sample mounting. As three-dimensional

https://doi.org/10.1017/S0033583520000128 Published online by Cambridge University Press

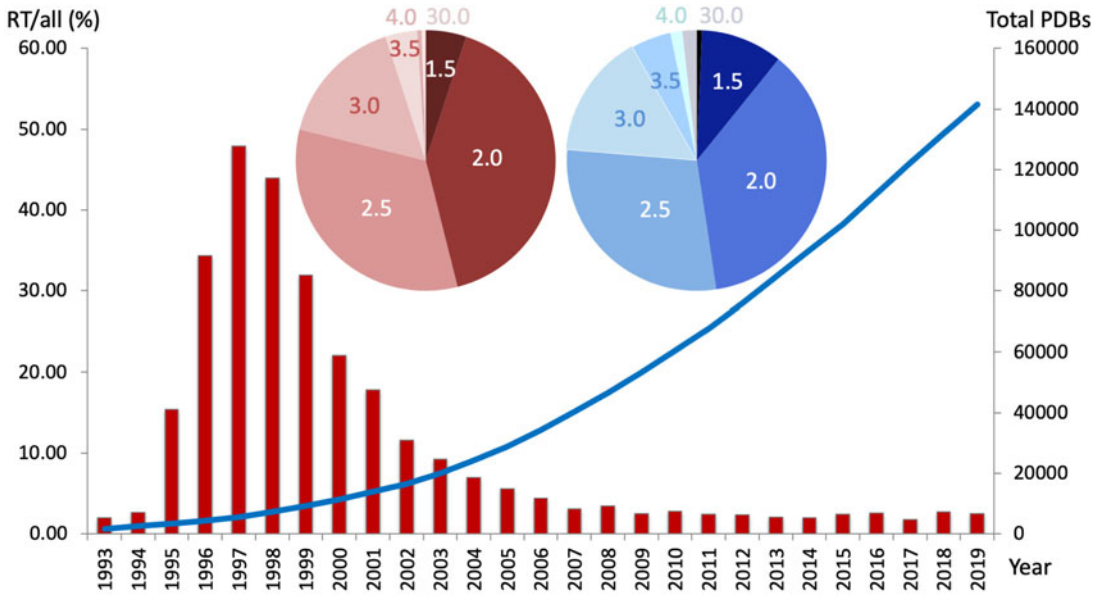

Fig. 1. The percentage of PDB datasets collected at room temperature (RT; 273–350 K) per year decreased steadily over the past 20 years (red bar graph, left *y*-axis), whereas the overall number of structures increased exponentially (blue line, right *y*-axis). Nearly 50% of all RTX structures were collected under 2.0 Å resolution, and over 75% were collected under 2.5 Å resolution. Cumulatively, approximately 94% of all deposited structures were collected at cryogenic temperatures. *Inset* – The distribution of resolutions (in Å) for RT structures (red pie chart) resembles the distribution of PDB structures collected at any temperature (blue pie chart).

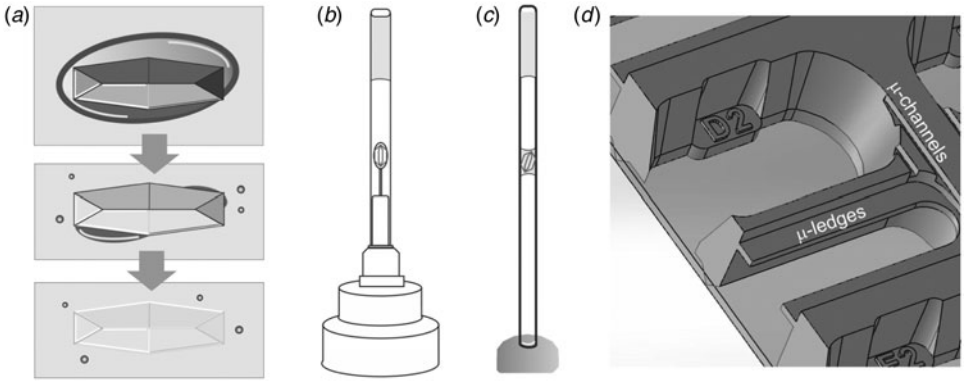

Fig. 2. BEFORE – Preparing macroscopic crystals for room temperature data collection. (*a*) Mother liquor (dark grey oval) surrounding a crystal in a large drop of oil (light grey box) is sequentially removed, leading to a visually 'disappearing' crystal due to the similar refractive indices of protein crystal and oil. (*b*) A mounted crystal is covered by a thin-walled polyester sleeve that contains a stabilizing solution. (*c*) In classic capillary mounting, the experimenter tries to achieve a solvent meniscus to hold the protein crystal in place. (*d*) MiTeGen's *In Situ*-1™ plate has microchannels and ledges that facilitate growing, shipping, and *in situ* data collection of crystals. A picture of the SSRL crystallization plate setup (Crystal Positioning Systems) can be found in the supplementary information of Martiel *et al.* (2019). For sample delivery methods of microcrystals that enable serial synchrotron crystallography see the section 'sample delivery for serial crystallography'.

(3D) printers become more accessible, custom 3D printed trays provide a viable alternative (Monteiro *et al.*, 2020).

If crystallization and travel kinetics are favorable, setting trays up locally is another option. However, this comes at the risk of wasting precious beamtime if crystallization does not turn out to be reproducible onsite. While this review focuses on macro-crystals of >100 µm, transferable sample delivery methods for microcrystals are emerging from efforts at X-ray free-electron laser facilities (XFEL). The required slew of microcrystals can simply be transported in a test tube to a suitable microfocus beamline that is equipped with a sample delivery option – reviewed below in the section 'sample delivery for serial crystallography'.

Mitigating dehydration

Oils

Before carefully handling crystals at the synchrotron, two major crystal killers need to be considered: dehydration and radiation damage (Atakisi *et al.*, 2018). First, dehydration is time-dependent, so working fast but gently is crucial. Oils can buy time. Oils that reduce crystal dehydration across a range of viscosities include Santovac 5®, NVH, Silicon Oil, Al's Oil, Paratone® N, and Paraffin Oil (Pflugrath, 2015). The crystal is either transferred into the oil directly or the oil is layered on top of the crystallization drop (Fig. 2*a*). Forming an oil seal that removes all contact between ambient air and the mother liquor can increase the working time from seconds to hours. The next step then becomes

https://doi.org/10.1017/S0033583520000128 Published online by Cambridge University Press

transferring crystals through the liquid–liquid interface between mother liquor and oil. One successful method is to stir the liquid–liquid mixture to remove most of the external mother liquor from the crystal. To get rid of stubborn solvent droplets, stir vigorously, close to the crystal or dislodge remaining droplets with a microtool, e.g., a MicroChisel^{TM} (MiTeGen). Note that crystals rarely physically disappear when they are transferred to the oil. Rather, the eye is misled by the similar refractive index of oil and protein, especially when the solvent layer is stripped off the surface (Warkentin and Thorne, 2009). A polarizing filter can often reveal the crystals that may have appeared to 'dissolve' or are hiding in the corners of the optically distorted drop (Fig. 2*a*). The final and equally important step is to remove excess oil from around the harvested crystal because the background created by any oil in the X-ray beam is comparable to that of an equal path through the protein crystal itself. An exception is oils containing heavier elements, such as silicon or fluorine, which scatter and absorb much more than a metal-free protein crystal. On the other hand, a layer of oil that is too thin can result in the aqueous phase poking through the oil. This promotes dehydration or surface tension, damaging the crystal lattice and causing poor diffraction. If crystal damage occurs despite the above measures, consider whether oil-soluble, volatile components of the mother liquor may evaporate and optimize conditions using different oils mentioned above. Getting the right amount of oil around the crystal is most easily achieved by touching the oil envelope to a clean surface or by using a paper wick (Hampton Research, Aliso Viejo, CA). If the crystal escapes the loop during the touch-off process it can simply be picked up again, taking advantage of the exceptionally long working time of oil-clad crystals. It is worth considering that anything other than the crystal in the beam dampens its diffraction: glass is the least transmissive, air is the most transmissive. Different plastics found in *in situ* trays, seals, loops, or sleeves differ in the magnitude and position of the ring of background that decreases the signal-to-noise ratio of specific resolution ranges. Consult the 'shadow' on the diffraction image, processing statistics, or a knowledgeable beamline scientist for insights.

One common myth is that thermal heating from the incident X-ray beam contributes to excess damage of the crystal by increasing reaction rates and evaporation. The contribution of hydrogen (H_2) or carbon dioxide (CO_2) gas has been discussed (Garman, 2010). H_2 gas forms when X-rays react with water and resulting H_2 bubbles cause physical distress to the crystal, distort the crystal lattice, and induce disorder that leads to fading high-resolution information (Meents *et al.*, 2010). In practice, this would suggest that retaining some mother liquor around the crystal may be beneficial to compensate for the release of the gas bubble. On the other hand, the radiolysis of water leads to hydroxyl and peroxide radicals that modify amino acids in order of their reactivity (Maleknia *et al.*, 1999). Others have discounted the causation of H_2 gas-induced radiation damage at higher temperatures (Warkentin and Thorne, 2010).

Capillaries

Capillaries are an alternative method to prevent crystal dehydration. Traditional mounting of crystals in borosilicate glass or quartz capillaries is remarkably watertight but can be difficult to master (King, 1954; Basavappa *et al.*, 2003). The mechanical stress of mounting a flat crystal onto the curved inner surface of a capillary is also not to be underestimated. Curvature incompatibilities were avoided in a contraption that resembles the 'grandfather' of the MiTeGen sleeve, which was used to study the stress-induced modulation of the soybean lipoxygenase L3 structure (Skrzypczak-Jankun *et al.*, 1996). However, the biggest disadvantage of quartz and glass capillary mounts is absorption. Per unit volume, glass scatters and absorbs roughly 10× that of the protein crystal itself. Therefore, for a 100 µm crystal, a 10 µm glass window starts to dominate the noise in the experiment. MiTeGen has now largely supplanted this method with a handy polyester tubing (Kalinin *et al.*, 2005) (Fig. 2*b*). Polyester, and indeed most plastics, scatter and absorb about as much as the same volume of protein, so the trade-off in thickness is much more forgiving. To stabilize fragile crystals, approximately 10 µl of environment-stabilizing solution (mother liquor or well solution) is injected into the sealed end of the 25 µm transparent polyester tube by using a gel-loading tip (Fig. 3). In fact, vapor diffusion can be used favorably to equilibrate the humidity inside the tube by using a mix that is compatible with the protein, such as 80% mother liquor to 20% water. The tube can be cut to size with a razor blade (it does not shatter like 10 µm glass capillaries) while reducing background scatter by about 60%. The crystal is then harvested with a loop that matches its size (Fig. 3*a*). Excess liquid is removed and the polyester tubing is drawn over the pin that holds the crystal, either with a steady hand or with the help of the MicroRT^{TM} Aligner (MiTeGen). The base can be additionally sealed with Dow Corning High-Vacuum Grease, which mitigates most evaporation except the approximately 80 nL h^{-1} that evaporates through the thin polyester tubing.

Data collection on bare crystals without protective sleeve shielding may be facilitated by humidity-control devices such as the original Proteros Free Mounting System (Kiefersauer *et al.*, 2000). To address the problem of dehydration, several European synchrotrons have formed a collaboration to implement a designated humidity-control device – the HC1 Dehydration Device (Sanchez-Weatherby *et al.*, 2009; Russi *et al.*, 2011). The commercial version HC-Lab Humidity Controller (Arinax) is used across many European synchrotrons and at the SSRL (Stanford, USA). Although initially used for controlled crystal dehydration, humidity control devices were adopted to replace the cryojet during RT data collection. Excess mother liquor around crystals that are harvested onto MicroMeshes (MiTeGen) can be wicked away from the other side of the mesh support, even when they are mounted in the humidity stream. At the bench, the humid-air and glue-coating method (Baba *et al.*, 2019) and MiTeGen's commercial solution, Watershed^{TM}, provide custom benchtop workstations to prevent drop dehydration during handling.

Avoiding cryoprotectants is another benefit of RTX data collection. Cryoprotectants often need to be optimized to obtain high-resolution data (Juers *et al.*, 2018). At high concentrations, fragment-sized cryoprotectants (like glycerol) are often found in protein structures. In a cautionary tale, Aggarwal *et al.* (2013) investigated the effect of cryoprotectants on carbonic anhydrase II. They found that, although neither protein thermostability nor the inhibitor binding are affected, glycerol does affect the kinetics of carbonic anhydrase II, presumably by displacing active-site solvent.

Reducing radiation damage

The other major crystal killer is radiation damage. At RT, radiation damage is time-dependent and mainly depends on flux density (Southworth-Davies *et al.*, 2007; Warkentin *et al.*, 2011, 2013). Dark progression, i.e., the progression of damage to the

https://doi.org/10.1017/S0033583520000128 Published online by Cambridge University Press

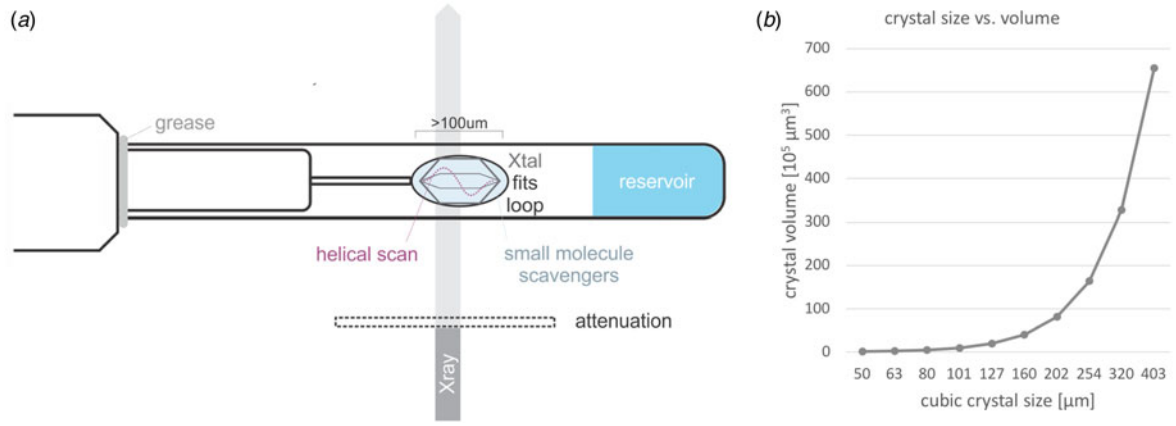

Fig. 3. DURING – Considerations for collecting room temperature data. (*a*) At RT, a protein crystal is mounted in a size-matched loop and protected from dehydration by a sleeve filled with reservoir solution. To reduce radiation damage, data are collected with an attenuated beam and potentially from different parts of the crystal using a helical scan or stepwise increments; small-molecule scavengers may help protect the crystal from radicals formed during data collection. (*b*) The crystal volume doubles with each increase in crystal size indicated on the *x*-axis for a cubic crystal; e.g. a crystal of 101 × 101 × 101 µm has twice the volume of a crystal of 80 × 80 × 80 µm. Note that in practice such crystals are often visually indistinguishable.

crystal after the X-rays have been turned off (Blundell and Johnson, 1976), was observed at temperatures above 180 K on timescales of 3–20 min (Warkentin *et al.*, 2011). The use of small-molecule radical scavengers, such as substituted benzoquinones [see (Allan *et al.*, 2013) for an extensive list], can mitigate radiation damage during data collection (De la Mora *et al.*, 2011) (Fig. 3). Unfortunately, none of these protective effects is very large. An improvement by a factor of two or more would be enough to overcome sample-to-sample variability and inspire a change in data collection strategy, but a reproducible demonstration of such a large radiation protection factor has yet to be reported. Exceptions to this rule are ultrafast X-ray pulses produced at XFELs where a diffraction pattern is produced before the structure can react to radiation exposure (Chapman, 2019). At RT the experimental limit of radiation damage is typically less than 400 kGy (Schubert *et al.*, 2016; De la Mora *et al.*, 2020), which is about one to two orders of magnitude lower than at cryo where the calculated Henderson limit is 20 MGy (Henderson, 1990; Nave and Garman, 2005; Garman and Owen, 2006) and the upper experimental limit is 30 MGy (Owen *et al.*, 2006). In practice, values vary considerably depending on the diffraction limit and chemical composition of the sample and dose rate (Teng and Moffat, 2000; Liebschner *et al.*, 2015; Atakisi *et al.*, 2019; Ebrahim *et al.*, 2019*b*). A more elaborate crystal lifetime estimator, RADDOSE-3D, that considers some of these factors are presented in the section 'optimizing data collection parameters'. Considering a practical RT limit of 400 kGy provides a rough guideline for expected crystal lifetime, required beam attenuation during RT data collection, or whether data merging to improve data completeness may be advisable (see the section 'collecting and merging data from multiple crystals'). Typically, R_{merge} values of less than 10% indicate that damage-induced changes are significantly smaller than the modeling error represented by R_{work} and R_{free} (Fraser *et al.*, 2011).

During: how to collect RTX data

Optimizing data collection parameters

During data collection, it is key to strike the balance between crystal lifetime and crystal diffraction. Intense beams produce more intense spots at high resolution but kill crystals faster. In turn, crystals survive much longer in attenuated beams but may not reach their full diffractive potential. An ideal data collection strategy maximizes diffraction to high resolution at high redundancy before the crystal suffers from radiation damage. In practice, the best way to approach this optimum is through trial and error, and focusing on a couple of parameters that increase the odds of squeezing the best data out of the crystal (Krojer *et al.*, 2013). First, match the crystal to the beam size or *vice versa* (i.e., adjust the beam aperture) to optimize the signal-to-noise ratio. Generally, exposing a larger crystal volume to the same X-ray dose fares better because of the number of molecules exposed to the beam scales with volume – by the third power of its linear size (Fig. 3*b*). For example, the volume, and hence the number of useful photons, double for two visually indistinguishable crystals of 80 and 101 µm (Holton, 2009).

Second, the beam can be attenuated by various means. The simplest way is to add an aluminum filter that attenuates the beam to a set percentage and extends crystal lifetime. By using attenuation, diffraction data can be collected at a slower rate for the same X-ray dose, which has the advantage of reducing the impact of time-dependent errors, such as beam flicker, shutter jitter, and the approximately 2 ms read-out gap between images of a PILATUS (Dectris) detector. It is important to familiarize oneself with the X-ray beam properties at each beamline. The beamline scientists should be able to provide information about the X-ray dose at different energies and beam sizes. Top-off mode of modern synchrotron sources, shutterless data collection with Pixel Array Detectors (PAD) and reduced dark time of faster PADs such as the EIGER or PILATUS (Dectris) enable faster data collection rates with good statistics (Rajendran *et al.*, 2011; Owen *et al.*, 2014). Fine-slicing data collection (Pflugrath, 1999; Krojer *et al.*, 2013) reduces spot overlap and allows more precise truncation of data once datasets fall below an acceptable threshold for radiation damage and resolution. If needed, a beamline scientist can advise how to explore other methods of reducing flux density that can improve the beam characteristics and hence data quality. These include the following: lowering the divergence will make the spots on the detector smaller and sharper; lowering the dispersion or bandpass can improve high-angle spot shape; and de-focusing the beam will lower the dose profile across the crystal

https://doi.org/10.1017/S0033583520000128 Published online by Cambridge University Press

face and minimize lattice strain propagating to nearby areas. The RADDOSE-3D calculator can help to predict the lifetime of protein crystals (Zeldin *et al.*, 2013*a*) and estimate the effective X-ray dose the crystal has endured during data collection (Zeldin *et al.*, 2013*b*; Bury *et al.*, 2018). Ideally, a 'top hat' beam profile enables homogeneous sample exposure and better assessment of the damage. Recently, the B_{Damage} metric was introduced to identify potential sites of specific damage by comparing the atomic B-factors of atoms with a similar local packing density environment (Gerstel *et al.*, 2015). For guidance on radiation damage that informs the practicalities of data collection, consult Holton's review and references therein (Holton, 2009).

Third, to counter fading peak intensities, consider collecting data from different parts of the crystal by translating (manually or automatically in segments) or helically scanning the crystal along the goniometer axis (Fig. 3). Grid scans on crystals have indicated that crystal quality is often heterogeneous (Thompson *et al.*, 2018). Collecting data from multiple crystals is another option discussed below.

Collecting and merging data from multiple crystals

Another prevailing RTX myth is that many crystals are needed to collect one complete dataset at RT. However, we routinely collect single crystal RTX datasets without radiation damage impeding electron density map interpretation or resulting in a dramatic decay in resolution (Fischer *et al.*, 2015). For samples where crystal damage due to dehydration or radiation damage is unavoidable, combining partial data from multiple crystals is an option. To obtain a dataset with desirable redundancy and completeness, multiple 'wedges' of data collected from often random orientations of multiple isomorphous crystals need to be merged. Redundancy increases accuracy, whereas completeness is needed for reliable model building and refinement. Since all reflections contribute to the electron density map, incomplete data lead to poor map quality (Wlodawer *et al.*, 2008). While spot indexing and integration usually work well if a sufficient number of spots with high signal-to-noise ratios are recorded, merging can be challenging. Luckily, RTX data are usually more isomorphous than cryogenic datasets (Giordano *et al.*, 2012), leading to better statistics and final models (Fischer *et al.*, 2015). Manual merging can be tedious as it requires human intervention by cycling between integrated and scaled data and monitoring the merging statistics to decide which data to include or exclude (Evans, 2006). The BLEND algorithm uses clustering based on unit cell parameters to facilitate the selection of optimal groups of multi-crystal data for scaling to achieve high completeness (Foadi *et al.*, 2013). When executed in 'graphics mode', annotated dendrograms with merging statistics can be displayed and inspected. Excluding the last recorded segments of the data that have suffered obvious radiation damage will help improve merging statistics and success. Conveniently, BLEND is also integrated into DIALS (Winter *et al.*, 2018; Beilsten-Edmands *et al.*, 2020), a collaborative software suite that provides a framework to automate processing diffraction images into MTZ files. Another program that uses hierarchical clustering from multi-crystal experiments is ccCluster, which also features an interactive graphical user interface for the analysis of dendrograms (Santoni *et al.*, 2017). Local scaling, dataset weighting, and merging data from multiple data files are also implemented in the *phenix.scale_and_merge* tool (Akey *et al.*, 2016) within Phenix (Liebschner *et al.*, 2019). Finally, it is worth noting that the nature of the intensity decay is different at cryo *versus* RT (De la Mora *et al.*, 2020). At cryo, high-resolution reflection intensities decay first as lattice strain increases. At RT all intensities appear to fade at once as the crystal lattice transitions to non-crystallinity, Wilson B-factors increase, and scattering power is lost (Leal *et al.*, 2013). Specific and global radiation damage are less decoupled at RT than at cryo, where specific damage affects certain amino acids (Gotthard *et al.*, 2019).

Sample delivery for serial crystallography

While this review focuses on collecting data on larger crystals, an emerging RTX trend is serial crystallography in which thousands of diffraction images are collected on microcrystals (Beale *et al.*, 2019). Exposing each crystal only once mitigates radiation damage. In addition to the benefit of an undistorted RT image, time-resolved crystallography (Moffat, 1989) allows dynamic insights into protein function. Using XFELs, 'molecular movies' can be recorded with femtosecond time resolution (Chapman *et al.*, 2011; Chapman, 2019). However, with limited XFEL beamtime available, following dynamics at synchrotrons remains a viable alternative, while other options like microcrystal electron diffraction have not reached mainstream maturity (Wolff *et al.*, 2020).

At synchrotron sources with monochromatic beams, the time resolution is currently limited to millisecond timescales (Stellato *et al.*, 2014; Nogly *et al.*, 2015; Jaeger *et al.*, 2016; Weinert *et al.*, 2017). Synchrotrons with a polychromatic 'pink' beam offer increased photon flux and 100 ps X-ray pulse exposures (Meents *et al.*, 2017; Martin-Garcia *et al.*, 2019). The promise of the 'pink' beam to accelerate serial crystallography is offset by higher backgrounds and less straightforward data processing (Förster and Schulze-Briese, 2019). Creative ways to deposit microcrystals into the X-ray beam in random orientations are increasing steadily. While most of these were originally developed for XFEL beamlines, many are amenable to being adapted by microfocus synchrotron beamlines. These include high-viscosity injection (Botha *et al.*, 2015; Nogly *et al.*, 2015; Kovácsová *et al.*, 2017; Martin-Garcia *et al.*, 2017), flowing crystals through quartz capillaries (Stellato *et al.*, 2014), low sample consumption microfluidic flow-focusing (Pawate *et al.*, 2015; de Wijn *et al.*, 2019; Monteiro *et al.*, 2019) using 3D printed devices (Monteiro *et al.*, 2020) and stable ultrasonic acoustic levitation of microliter droplets (Tsujino and Tomizaki, 2016). Ongoing work addresses problems with clogging and flow-speed of microfluidics, bubble generation, viscous stream focusing, deposition of varied-sized crystals, and sample consumption to enable the routine, uninterrupted collection of serial crystallography data. Popular fixed-target approaches include *in situ* deposition of crystal-containing drops on a humidity-controlled hit-and-return chip (Baxter *et al.*, 2016; Mehrabi *et al.*, 2019*b*; Mehrabi *et al.*, 2020), sandwiched between mylar, kapton, or cyclic-olefin-copolymer foils (Schubert *et al.*, 2016; Broecker *et al.*, 2018; Doak *et al.*, 2018; Feiler *et al.*, 2019; Wierman *et al.*, 2019), on micropatterned silicon chips (Mueller *et al.*, 2015; Roedig *et al.*, 2016; Meents *et al.*, 2017; Owen *et al.*, 2017; Ebrahim *et al.*, 2019*a*) or transported into the beam by a conveyor-belt like tape drive (Roessler *et al.*, 2013; Beyerlein *et al.*, 2017). Another option is to directly grow crystals on an *in situ* micropatterned silicon chip. This minimizes crystal handling, allows the manipulation of sensitive crystals, and enables ligand soaking for serial crystallography (Lieske *et al.*, 2019). Predetermining crystal positions on the chip accelerates crystal

https://doi.org/10.1017/S0033583520000128 Published online by Cambridge University Press

alignment and improves hit rates under controlled humidity conditions (Oghbaey *et al*., 2016). For more detailed accounts on creative sample delivery systems refer to articles such as Martiel *et al.* (2019), Grünbein and Nass Kovacs (2019), Zhao *et al*. (2019), and references therein.

After: what to do with RTX data

One thing to note upon processing a RTX dataset is that the mosaicity is often less than that of comparable cryogenic datasets (Garman and Doublié, 2003; Moreau *et al*., 2019). Reduced mosaicity maximizes the data quality and resolution limit (Mitchell and Garman, 1994), thereby counteracting accelerated diffraction decay that decreases the resolution. Higher isomorphism among RTX datasets (Fischer *et al*., 2015) also enables the better merging of data from multiple crystals (see the section 'collecting and merging data from multiple crystals'). Provided that the data quality is high, resolutions of less than ∼1.8 Å are best to model alternative conformations. At lower than 2.5 Å, modeling alternative conformations is limited but conserved water molecules are still captured, whereas, with lower resolution, fewer alternative features will be accessible. However, we remain confident that the observed conformations in RTX data are undistorted by idiosyncrasies of the flash-cooling protocol. When processing RTX data, it is of utmost importance to track signs of radiation damage and conservatively cut the data accordingly (see the section 'reducing radiation damage'). Crystals with high symmetry reduce the amount of data that is needed to collect or increase redundancy. Accounting for radiation damage during and after data collection is crucial to ensure that the observed conformational variance is indeed caused by temperature and not by radiation damage (Russi *et al*., 2017).

Modeling heterogeneity

Resulting high-resolution RTX data have inspired the development of a set of new tools that assist refinement, modeling, and analysis of alternative conformations. Originally, in the context of collecting anomalous data, Diederichs *et al*. introduced a simple partial correction for intensity decay of reflections following radiation damage via a redundancy-based 'zero dose extrapolation' that leads to enhanced electron density maps (Diederichs *et al*., 2003). On the refinement end, available tools include qFit and Phenix. The qFit algorithm uses an iterative procedure to represent discrete heterogeneity by fitting multi-conformers that are commonly ignored during manual model building into electron density maps (Fig. 4*d*). Since its initial implementation, qFit has expanded from side-chain rotamers (van den Bedem *et al*., 2009) to backbone heterogeneity (Keedy *et al*., 2015*a*) and to ligands (van Zundert *et al*., 2018). The new release of qFit 3 expands the work into single-particle cryoEM density maps (Riley *et al*., 2020). Phenix offers occupancy-refinement and ensemble-refinement strategies based on time averaging of simple molecular dynamics simulations to model X-ray data better than single structures (Burnley *et al*., 2012). None of these automated methods is the panacea. They support rather than replace careful inspection of the electron density maps by an experienced crystallographer. Inspiration for modeling and analysis can also come from other helpful tools such as Ringer and CONTACT. Ringer is the quantitative, automated alternative to qualitative, manual inspection of electron density maps within Coot (Emsley *et al*., 2010). Ringer samples electron density maps around dihedral angles of each protein residue (Lang *et al*., 2010). Statistical evidence supports modeling of alternative conformations below the traditional 1 sigma cutoff, even down to about 0.3 sigma (Fig. 4*c*). The result is more reflective of the polymorphic nature of proteins than a single structure (Fraser *et al*., 2011). For those interested in allostery, the CONTACT algorithm identifies networks of correlated motions of conformationally heterogeneous residues (van den Bedem *et al*., 2013) (Fig. 4*e–f*). Sterically mutually exclusive placement of neighboring residues can form a functional network that links remote effector sites to the active site. The observation that such functional networks have been identified independently via co-evolving amino acids may present a framework to combine a phylogenetic with a dynamic view of protein evolvability (van den Bedem and Fraser, 2015).

Looking back and moving forward – lessons learned

I will close with several case studies in which RTX has recently contributed dynamic, high-resolution insights into the biophysics and function of soluble proteins and membrane-bound proteins (Martin-Garcia *et al*., 2017). These examples were selected as conceptual and experimental templates for the design of RT-inspired experiments, rather than to exhaustively review the depth and breadth of the available literature.

Integrated approaches

RTX studies have the most impact when they are used in combination with complementary methods to illuminate an unappreciated aspect of biological function. RTX studies of proline isomerase cyclophilin A (CypA) revealed hidden conformational states that are important for catalysis (Fraser *et al*., 2009). To populate this conformation, a mutation was designed that inverted the conformational states observed at equilibrium and correlated with catalytic rates of the enzyme. In combination with nuclear magnetic resonance (NMR) analysis, this demonstrated the strength of RTX in accessing functional protein dynamics. Correlation between fluctuations detected by NMR in solution and RT electron density maps were also discovered for the oncogenic-signaling switch protein Ras (Scheidig *et al*., 1999; Fraser *et al*., 2011). Revealing the structural origin for this allosteric network provided insights into a catalytically competent conformation of Ras that aids mechanistic understanding of Ras inhibition (Lu *et al*., 2016). Another powerful combination of methods at RT is joint X-ray/neutron refinement. Intricacies of H-bonding were revealed for several different proteins. A cGMP-dependent protein kinase joint X-ray/neutron refinement of RT data suggests that the conformation of an arginine interacting with cGMP is more dynamic than previously appreciated and it is 'frozen-out' in the low-temperature structure (Huang *et al*., 2014). The same group also discovered an unprecedented low-barrier H-bond in concanavalin A, a legume lectin with anticancer potential (Gerlits *et al*., 2017*b*). Another study found that interactions between an HIV protease triple-mutant with the inhibitor amprenavir are not as significantly altered as proposed on the basis of a cryogenic structure (Gerlits *et al*., 2017*a*). Most recently, RT neutron and X-ray data were collected on the main protease of SARS-CoV-2 (Kneller *et al*., 2020*a*) for which RT X-ray studies have revealed novel backbone conformations in the P5 binding pocket (Kneller *et al*., 2020*b*).

The comparison of structural ensembles of CypA collected at synchrotron and XFEL sources confirms the agreement between

https://doi.org/10.1017/S0033583520000128 Published online by Cambridge University Press

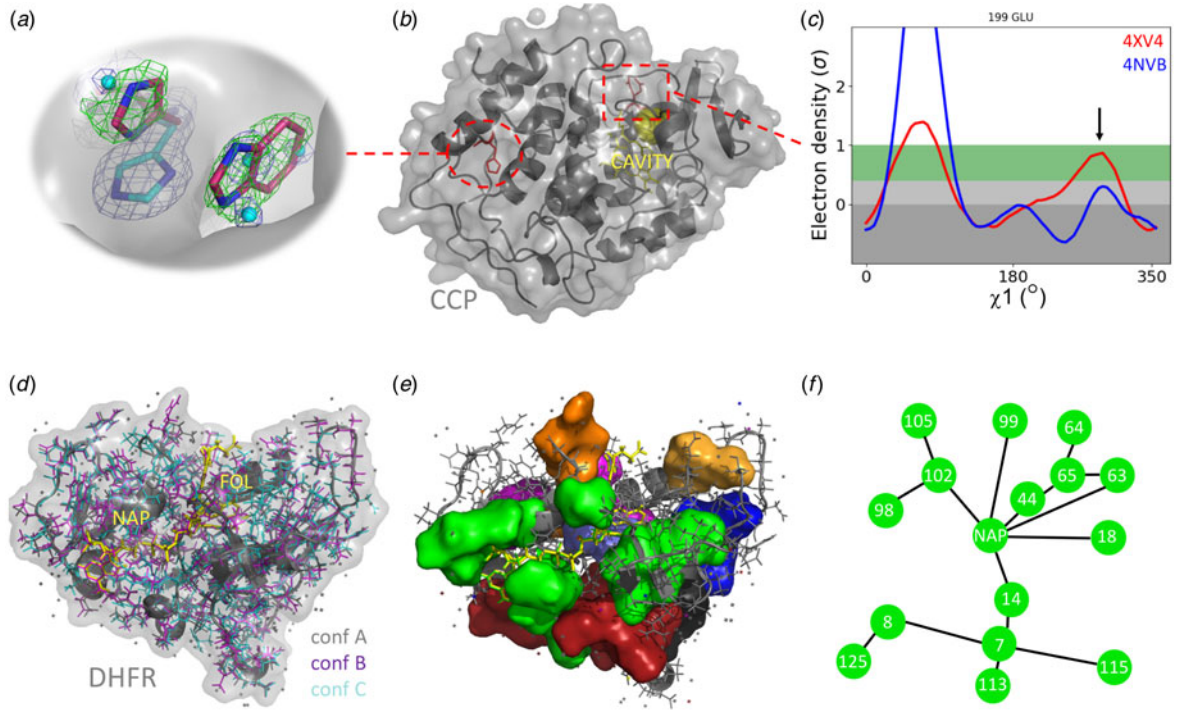

Fig. 4. AFTER – Working with room temperature data; exemplified for two proteins, cytochrome C peroxidase gateless mutant (CCP; panels *a*–*c*) and dihydrofolate reductase (DHFR; panels *d*–*f*). (*a*) Crystallographic data of CCP (grey surface) bound to benzimidazole were collected from the same crystal at RT (4xv5, red) and cryogenic temperature (4nve, cyan). Green difference electron density shows that only at RT does His96 occupy an alternative 'open' conformation, revealing a transient secondary site that is occupied by benzimidazole, whereas water occupies the 'closed' site at cryo. (*b*) Overview of CCP with the ligand cavity in yellow and distal cryptic site is highlighted by a red dashed ellipsoid. (*c*) Ringer plot of CCP bound to another ligand, 2-amino-5-methylthiazole, shows an alternate conformation of Glu199 near the cavity site at RT (red line) [below the common threshold of 1 sigma (Fraser *et al.*, 2011)] that is hidden at cryogenic temperature (blue line). (*d*) Multi-conformer model of DHFR built by qFit with alternate conformations B in magenta, C in cyan, and the $NADP^+$ cofactor (NAP) and folate (FOL) in yellow sticks. (*e*) Nine CONTACT networks are mapped onto the DHFR structure (in the same orientation as in *d*). (*f*) The largest network identified by CONTACT contains 15 residues (sequence numbers given in nodes) and the NAP ligand. Edges connect nodes of clashing residues that are relieved by alternative conformations.

both methods and motivates experiments that resolve the temperature- and time-coordinate of protein functional dynamics (Keedy *et al.*, 2015*b*). As this review focuses on synchrotron RTX, I refer to topical reviews that highlight the value of XFEL RT studies to investigate the important target class of membrane-associated proteins, such as Neutze *et al.* (2015), Martin-Garcia *et al.* (2016), Mishin *et al.* (2019), Wickstrand *et al.* (2019).

Variable temperature crystallography

Variable temperature crystallography uses discrete temperature steps to sample the protein conformational landscape (Keedy, 2019). Given the experimental obstacles, there are only a few examples of 'temperature titrations' since the pioneering efforts mentioned above (Frauenfelder *et al.*, 1979; Tilton *et al.*, 1992). A further two decades later, variable temperature crystallography was used to study the complex evolution of conformational heterogeneity for CypA across a range of eight temperatures. The authors found that instead of a single concerted movement across the protein, different parts of the protein have different transition temperatures (Keedy *et al.*, 2015*b*). Temperature changes have also been used to analyze flavodoxin oxidation states (Watt *et al.*, 1991), and the *in crystallo* thermodynamics of conformational states of a redox quinone co-factor in bacterial copper amine oxidase during the catalytic reaction (Murakawa *et al.*, 2019). Advances in collecting high-temperature datasets at 293–363 K promise future temperature explorations of the conformational landscape beyond proteinase K, thaumatin, and lysozyme (Doukov *et al.*, 2020).

Ligands

Conformational heterogeneity is present not only in protein structures but also in ligands. Ligands adopt a wide range of conformations upon binding to proteins. This is especially true for small-molecule fragments that bind with low affinity and high promiscuity. However, finding evidence for multiple binding modes within an averaged electron density map can be difficult. To address this shortcoming, qFit-ligand was developed to find often isoenergetic, unmodeled conformations of drug-like molecules within crystal structures (van Zundert *et al.*, 2018). For PDB structures of cancer target BRD4, the method revealed that as much as 29% of the protein crystal structures showed evidence of unmodeled protein–ligand interactions that would have been informative to guide compound design (Raich *et al.*, 2020). Generally, one rarely finds ligand sites 100% occupied, as they are typically modeled. Especially at RT, ligand binding is thermodynamically less favorable (Fischer *et al.*, 2015). Hence ligand complexes should be modeled as ensembles of bound and unbound states (Pearce *et al.*, 2017).

Computational ligand discovery struggles from weighting energy penalties of relevant conformational states when looking for ligands in large databases. In a study of model protein cytochrome C peroxidase, the RT structure of the apo state visualized three conformational states of the protein that could be used in

https://doi.org/10.1017/S0033583520000128 Published online by Cambridge University Press

docking (Fischer *et al.*, 2014). Their relative occupancies were used to calculate Boltzmann-weighted energy penalties in docking. Using this approach, the authors identified ligands that stabilized specific conformational states that would not have been identified at cryo. Furthermore, comparisons of pairwise cryo–RT datasets of protein-ligand complexes provided insights into systematic structural differences (Fischer *et al.*, 2015). For instance, side chains near the canonical ligand-binding site were remodeled in response to temperature (Fig. 4*c*). If only the cryo dataset was considered, as is common in computational drug discovery, these changes may have been mistaken for genuine responses to ligand binding, rather than temperature artifacts. Strikingly, the remodeling of a distal residue exposed a remote cryptic site that was hidden in the cryogenic structure collected on the same crystal (Fig. 4*a*).

Allostery and mutations

Allostery is often mediated by correlated motions across the protein (Mehrabi *et al.*, 2019b). The CONTACT algorithm capitalizes on the exchange between conformational substates that can be revealed in RTX electron density maps (van den Bedem *et al.*, 2013). In a study of *E. coli* dihydrofolate reductase, CONTACT recapitulated the effect of an allosteric mutation seen by NMR chemical-shift perturbations. This demonstrated that altering optimized contact networks of coordinated motions can impair catalytic function. In an endeavor to discover new allosteric sites for the diabetes target protein tyrosine phosphatase 1B, the active-site WPD loop opening was revealed at elevated temperatures (Keedy *et al.*, 2018). However, loop occupancies did not increase linearly with temperature. A new sample delivery system for serial RTX helped track long-range interactions and higher-energy conformations that appear to be critical for substrate access to the active site of trans-acyltransferase (Mathews *et al.*, 2017).

Like temperature and ligands, mutations represent another perturbation of protein structure. Such unintentional mutations may arise to confer resistance to anti-cancer, anti-bacterial, anti-viral, or anti-fungal treatment. Understanding the effect of mutation on protein structure is also key to intentionally inform protein engineering in the pursuit of guiding the design of new protein function. Laboratory evolution of protein function takes many rounds of optimization. During the initial directed evolution, using the increase in flexibility as a guide to escape local energy minima emerged as the most promising strategy to increase the binding affinity of redesigned ubiquitin variants to the deubiquitinase USP7 (Biel *et al.*, 2017). Other work on laboratory evolution of a designed Kemp eliminase used RTX to recapitulate shifts in the conformational ensemble towards catalytically-productive sub-states (Broom *et al.*, 2020). This suggests that RTX guided ensemble modeling can help inform directed evolution efforts. In a recent study, a combination of thermodynamic cycles and RTX was used to track perturbations in water networks. While delicate shifts in water positions are often ignored, introducing subtle changes in the protein and ligands demonstrated that water networks contribute substantially to the binding of congeneric sialic acid ligands to virulence protein SiaP (Darby *et al.*, 2019).

Conclusion and outlook

While the number of structures deposited in the PDB has increased exponentially over the past two decades, RT structures represent only a small fraction (~6%) of the more than 169 000 structures (as of October 2020). RTX has great potential to offer novel insights into protein structure and functional dynamics, complementary to cryogenic methods, which will undoubtedly persevere. By resolving several myths that deter most experimenters from conducting routine RTX data collection at synchrotrons, I want to facilitate the planning, collection, and interpretation of RTX data. Considering the method's merits, I hope to spark a renaissance in RTX methods, contrary to the trend observed in Fig. 1.

(Im)practicalities of RTX data collection include: Myth 1 – *Preparing for RTX data collection is tedious*. I laid out simple alternatives to preparing crystals for RTX data collection beyond tales of tedious capillary mounting. Myth 2 – *It is not possible to collect a complete dataset before radiation damage or dehydration destroys the crystal*. Using the experimental setup described above, we have on several occasions, and for unrelated proteins, successfully collected multiple consecutive datasets on a single protein crystal. Anecdotally, for cytochrome C peroxidase, we collected three complete consecutive datasets before the resolution fell below 2 Å and seven datasets before it was less than 3 Å (Fischer *et al.*, 2015). Reassuringly, with the right measures in place, protein conformational variation at RT is observed in spite of radiation damage and not as a result of it (Russi *et al.*, 2017; Gotthard *et al.*, 2019). Myth 3 – *One cannot collect high-resolution data at RT*. Remarkably, the distribution of resolutions of RT structures closely resembles that of all PDB structures (Fig. 1): about 50% of all RT structures are collected to less than 2 Å, and over 75% are collected to less than 2.5 Å resolution. Although one may argue a bias toward well-diffracting crystals, we find across diverse projects that sufficiently large (⩾100 µM), well-diffracting (<2 Å) crystals at cryogenic temperatures often achieve similar resolutions (±0.5 Å) at RT. For instance, we observed comparable average resolutions of 1.6 Å at RT and 1.4 Å at cryogenic temperature for six dataset pairs collected at both temperatures on the same crystal (Fischer *et al.*, 2015). Recent studies showed that RTX data collection is even amenable to 'difficult' crystals, like membrane proteins in the lipid cubic phase, which can diffract to <1.5 Å at RT as shown for the XFEL study on the influenza M2 proton channel (Thomaston *et al.*, 2017). Retrospectively, about twice as many cryo structures achieve resolutions <1.5 Å compared to those collected at RT (Fig. 1). However, we need not confuse precision with accuracy – despite increased chances for high resolution diffraction at cryo, residues may still be distorted or missed entirely as discussed above.

It is worth reiterating that despite the promise of dynamic insights gained, radiation damage can limit or mislead model interpretation, even at very low absorbed doses for radiation-sensitive proteins (Ebrahim *et al.*, 2019*b*). Careful planning and execution of experiments is crucial to avoid general (Holton, 2009) and specific (Garman and Weik, 2017) radiation damage at any temperature, but cryogenic data are more forgiving by a couple orders of magnitude (see the section 'reducing radiation damage'). Merging data from multiple isomorphous crystals allows discarding those segments of data from each crystal that are compromised by radiation damage and assemble data from several crystals into a complete, undamaged data set (see the section 'collecting and merging data from multiple crystals'). Nonetheless, several examples demonstrate that structural models at RT provide new insights into protein dynamics underlying function (Fraser *et al.*, 2009), ligand binding and discovery (Fischer *et al.*, 2014, 2015), and water dynamics (Thomaston

https://doi.org/10.1017/S0033583520000128 Published online by Cambridge University Press

et al., 2017; Darby *et al.*, 2019), with many opportunities to extend into other fields like protein engineering and design (Biel *et al.*, 2017; Broom *et al.*, 2020). Ongoing methodological advances will further bolster the ability to collect physiologically relevant data (Helliwell, 2020) at synchrotrons and XFELs.

One can imagine changing other variables despite temperature to perturb the protein conformational landscape such as pH (Socher and Sticht, 2016), humidity (Sanchez-Weatherby *et al.*, 2009; Douangamath *et al.*, 2013), substrates (Schmidt, 2013; Mehrabi *et al.*, 2019*a*), pressure (Collins *et al.*, 2011), electric field pulses (Hekstra *et al.*, 2016), time (Schulz *et al.*, 2018), ionic strength, oxygen, co-factors etc. – either individually or in combination. The key will be to disentangle the range of induced changes and link them to functional consequences via the integration of complementary methods and development of new collection and analysis schemes.

In the process of leveraging the potential of RTX it is important to strike a fine balance: resist the temptation of hastily drawing functional conclusions but explore ways to pragmatically use and synergistically complement RTX dynamic information. For instance, while computational docking implementations routinely discard carefully modeled alternative states in 'preparation' for virtual library screens, RTX data have been useful to inform energy penalties in ligand discovery (Fischer *et al.*, 2014). Likewise, computational methods on the other end of the speed-*versus*-accuracy continuum, such as free-energy-of-binding calculations, may benefit from RTX input. The most powerful implementation is an integrated approach, where RTX is combined with complementary dynamic methods such as NMR (Henzler-Wildman and Kern, 2007; Fenwick *et al.*, 2014), single-molecule FRET microscopy (Juette *et al.*, 2014; Borgia *et al.*, 2018), molecular simulations (Bowman *et al.*, 2014; Bottaro and Lindorff-Larsen, 2018), diffuse scattering (Wall *et al.*, 2014; Meisburger *et al.*, 2017), and hydrogen-deuterium exchange mass spectrometry (Oganesyan *et al.*, 2018; Masson *et al.*, 2019) to better characterize the protein conformational landscape of functionally relevant motions. Even for well-studied biomolecules, an integrative dynamic view of protein function will advance basic and biomedical research.

Acknowledgements. I thank Dr. AJ McArthur and CM Fischer for critical reading of the manuscript, and Drs. JS Fraser, JM Holton and RA Nicholls for insightful discussions. This work was supported by ALSAC, St. Jude Children's Research Hospital.

Conflict of interest. None to declare.

References

Aggarwal M, Boone CD, Kondeti B, Tu C, Silverman DN and Mckenna R (2013) Effects of cryoprotectants on the structure and thermostability of the human carbonic anhydrase II-Acetazolamide complex. *Acta Crystallographica. Section D, Biological Crystallography* **69**(Pt 5), 860–865.

Akey DL, Terwilliger TC and Smith JL (2016) Efficient merging of data from multiple samples for determination of anomalous substructure. *Acta Crystallographica. Section D, Structural Biology* **72**(Pt 3), 296–302.

Alcorn T and Juers DH (2010) Progress in rational methods of cryoprotection in macromolecular crystallography. *Acta Crystallographica. Section D, Biological Crystallography* **66**(Pt 4), 366–373.

Allan EG, Kander MC, Carmichael I and Garman EF (2013) To scavenge or not to scavenge, that is STILL the question. *Journal of Synchrotron Radiation* **20**(Pt 1), 23–36.

Atakisi H, Moreau DW and Thorne RE (2018) Effects of protein-crystal hydration and temperature on side-chain conformational heterogeneity in monoclinic lysozyme crystals. *Acta Crystallographica. Section D, Structural Biology* **74**(Pt 4), 264–278.

Atakisi H, Conger L, Moreau DW and Thorne RE (2019) Resolution and dose dependence of radiation damage in biomolecular systems. *IUCrJ* **6**(Pt 6), 1040–1053.

Baba S, Shimada A, Mizuno N, Baba J, Ago H, Yamamoto M and Kumasaka T (2019) A temperature-controlled cold-gas humidifier and its application to protein crystals with the humid-air and glue-coating method. *Journal of Applied Crystallography* **52**(Pt 4), 699–705.

Basavappa R, Petri ET and Tolbert BS (2003) A quick and gentle method for mounting crystals in capillaries. *Journal of Applied Crystallography* **36**, 1297–1298.

Baxter EL, Aguila L, Alonso-Mori R, Barnes CO, Bonagura CA, Brehmer W, Brunger AT, Calero G, Caradoc-Davies TT, Chatterjee R, Degrado WF, Fraser JS, Ibrahim M, Kern J, Kobilka BK, Kruse AC, Larsson KM, Lemke HT, Lyubimov AY, Manglik A, Mcphillips SE, Norgren E, Pang SS, Soltis SM, Song J, Thomaston J, Tsai Y, Weis WI, Woldeyes RA, Yachandra V, Yano J, Zouni A and Cohen AE (2016) High-density grids for efficient data collection from multiple crystals. *Acta Crystallographica. Section D, Structural Biology* **72**(Pt 1), 2–11.

Beale JH, Bolton R, Marshall SA, Beale EV, Carr SB, Ebrahim A, Moreno-Chicano T, Hough MA, Worrall JAR, Tews I and Owen RL (2019) Successful sample preparation for serial crystallography experiments. *Journal of Applied Crystallography* **52**(Pt 6), 1385–1396.

Beilsten-Edmands J, Winter G, Gildea R, Parkhurst J, Waterman D and Evans G (2020) Scaling diffraction data in the DIALS software package: algorithms and new approaches for multi-crystal scaling. *Acta Crystallographica. Section D, Structural Biology* **76**(Pt 4), 385–399.

Beyerlein KR, Dierksmeyer D, Mariani V, Kuhn M, Sarrou I, Ottaviano A, Awel S, Knoska J, Fuglerud S, Jönsson O, Stern S, Wiedorn MO, Yefanov O, Adriano L, Bean R, Burkhardt A, Fischer P, Heymann M, Horke DA, Jungnickel KEJ, Kovaleva E, Lorbeer O, Metz M, Meyer J, Morgan A, Pande K, Panneerselvam S, Seuring C, Tolstikova A, Lieske J, Aplin S, Roessle M, White TA, Chapman HN, Meents A and Oberthuer D (2017) Mix-and-diffuse serial synchrotron crystallography. *IUCrJ* **4**(Pt 6), 769–777.

Biel JT, Thompson MC, Cunningham CN, Corn JE and Fraser JS (2017) Flexibility and design: conformational heterogeneity along the evolutionary trajectory of a redesigned ubiquitin. *Structure (London, England: 1993)* **25**, 739–749.e733.

Blundell TL and Johnson LN (1976) *Protein Crystallography*. London: Academic Press.

Borgia A, Borgia MB, Bugge K, Kissling VM, Heidarsson PO, Fernandes CB, Sottini A, Soranno A, Buholzer KJ, Nettels D, Kragelund BB, Best RB and Schuler B (2018) Extreme disorder in an ultrahigh-affinity protein complex. *Nature* **555**, 61–66.

Botha S, Nass K, Barends TR, Kabsch W, Latz B, Dworkowski F, Foucar L, Panepucci E, Wang M, Shoeman RL, Schlichting I and Doak RB (2015) Room-temperature serial crystallography at synchrotron X-ray sources using slowly flowing free-standing high-viscosity microstreams. *Acta Crystallographica. Section D, Biological Crystallography* **71**(Pt 2), 387–397.

Bottaro S and Lindorff-Larsen K (2018) Biophysical experiments and biomolecular simulations: a perfect match? *Science (New York, N.Y.)* **361**, 355–360.

Bowman GR, Pande VS and Noé F (2014) *An introduction to Markov State Models and Their Application to Long Timescale Molecular Simulation*. Springer Netherlands.

Broecker J, Morizumi T, Ou WL, Klingel V, Kuo A, Kissick DJ, Ishchenko A, Lee MY, Xu S, Makarov O, Cherezov V, Ogata CM and Ernst OP (2018) High-throughput *in situ* X-ray screening of and data collection from protein crystals at room temperature and under cryogenic conditions. *Nature Protocols* **13**, 260–292.

Broom A, Rakotoharisoa RV, Thompson MC, Zarifi N, Nguyen E, Mukhametzhanov N, Liu L, Fraser JS and Chica RA (2020) Ensemble-based enzyme design can recapitulate the effects of laboratory directed evolution in silico. *Nature Communications* **11**, 4808.

Burley SK, Berman HM, Christie C, Duarte J, Feng Z, Westbrook J, Young J and Zardecki C (2018) RCSB Protein Data Bank: sustaining a living dig-

https://doi.org/10.1017/S0033583520000128 Published online by Cambridge University Press

ital data resource that enables breakthroughs in scientific research and biomedical education. *Protein Science* **27**, 316–330.

Burnley BT, Afonine PV, Adams PD and Gros P (2012) Modelling dynamics in protein crystal structures by ensemble refinement. *Elife* **1**, e00311.

Bury CS, Brooks-Bartlett JC, Walsh SP and Garman EF (2018) Estimate your dose: RADDOSE-3D. *Protein Science* **27**, 217–228.

Chapman HN (2019) X-ray free-electron lasers for the structure and dynamics of macromolecules. *Annual Review of Biochemistry* **88**, 35–58.

Chapman HN, Fromme P, Barty A, White TA, Kirian RA, Aquila A, Hunter MS, Schulz J, Deponte DP, Weierstall U, Doak RB, Maia FR, Martin AV, Schlichting I, Lomb L, Coppola N, Shoeman RL, Epp SW, Hartmann R, Rolles D, Rudenko A, Foucar L, Kimmel N, Weidenspointner G, Holl P, Liang M, Barthelmess M, Caleman C, Boutet S, Bogan MJ, Krzywinski J, Bostedt C, Bajt S, Gumprecht L, Rudek B, Erk B, Schmidt C, Hömke A, Reich C, Pietschner D, Strüder L, Hauser G, Gorke H, Ullrich J, Herrmann S, Schaller G, Schopper F, Soltau H, Kühnel KU, Messerschmidt M, Bozek JD, Hau-Riege SP, Frank M, Hampton CY, Sierra RG, Starodub D, Williams GJ, Hajdu J, Timneanu N, Seibert MM, Andreasson J, Rocker A, Jönsson O, Svenda M, Stern S, Nass K, Andritschke R, Schröter CD, Krasniqi F, Bott M, Schmidt KE, Wang X, Grotjohann I, Holton JM, Barends TR, Neutze R, Marchesini S, Fromme R, Schorb S, Rupp D, Adolph M, Gorkhover T, Andersson I, Hirsemann H, Potdevin G, Graafsma H, Nilsson B and Spence JC (2011) Femtosecond X-ray protein nanocrystallography. *Nature* **470**, 73–77.

Collins MD, Kim CU and Gruner SM (2011) High-pressure protein crystallography and NMR to explore protein conformations. *Annual Review of Biophysics* **40**, 81–98.

Darby JF, Hopkins AP, Shimizu S, Roberts SM, Brannigan JA, Turkenburg JP, Thomas GH, Hubbard RE and Fischer M (2019) Water networks can determine the affinity of ligand binding to proteins. *Journal of the American Chemical Society* **141**, 15818–15826.

De la Mora E, Carmichael I and Garman EF (2011) Effective scavenging at cryotemperatures: further increasing the dose tolerance of protein crystals. *Journal of Synchrotron Radiation* **18**(Pt 3), 346–357.

De la Mora E, Coquelle N, Bury CS, Rosenthal M, Holton JM, Carmichael I, Garman EF, Burghammer M, Colletier JP and Weik M (2020) Radiation damage and dose limits in serial synchrotron crystallography at cryo- and room temperatures. *Proceedings of the National Academy of Sciences of the United States of America* **117**, 4142–4151.

De Wijn R, Hennig O, Roche J, Engilberge S, Rollet K, Fernandez-Millan P, Brillet K, Betat H, Mörl M, Roussel A, Girard E, Mueller-Dieckmann C, Fox GC, Olieric V, Gavira JA, Lorber B and Sauter C (2019) A simple and versatile microfluidic device for efficient biomacromolecule crystallization and structural analysis by serial crystallography. *IUCrJ* **6**(Pt 3), 454–464.

Diederichs K, McSweeney S and Ravelli RB (2003) Zero-dose extrapolation as part of macromolecular synchrotron data reduction. *Acta Crystallographica. Section D, Biological Crystallography* **59**(Pt 5), 903–909.

Ding X, Rasmussen BF, Petsko GA and Ringe D (2006) Direct crystallographic observation of an acyl-enzyme intermediate in the elastase-catalyzed hydrolysis of a peptidyl ester substrate: exploiting the "glass transition" in protein dynamics. *Bioorganic Chemistry* **34**, 410–423.

Doak RB, Nass Kovacs G, Gorel A, Foucar L, Barends TRM, Grünbein ML, Hilpert M, Kloos M, Roome CM, Shoeman RL, Stricker M, Tono K, You D, Ueda K, Sherrell DA, Owen RL and Schlichting I (2018) Crystallography on a chip – without the chip: sheet-on-sheet sandwich. *Acta Crystallographica. Section D, Structural Biology* **74**(Pt 10), 1000–1007.

Douangamath A, Aller P, Lukacik P, Sanchez-Weatherby J, Moraes I and Brandao-Neto J (2013) Using high-throughput *in situ* plate screening to evaluate the effect of dehydration on protein crystals. *Acta Crystallographica. Section D, Biological Crystallography* **69**(Pt 5), 920–923.

Doukov T, Herschlag D and Yabukarski F (2020). A robust method for collecting X-ray diffraction data from protein crystals across physiological temperatures. *bioRxiv*, 2020·2003·2017·995852.

Drew HR, Samson S and Dickerson RE (1982) Structure of a B-DNA dodecamer at 16 K. *Proceedings of the National Academy of Sciences of the United States of America* **79**, 4040–4044.

Ebrahim A, Appleby MV, Axford D, Beale J, Moreno-Chicano T, Sherrell DA, Strange RW, Hough MA and Owen RL (2019*a*) Resolving polymorphs and radiation-driven effects in microcrystals using fixed-target serial synchrotron crystallography. *Acta Crystallographica. Section D, Structural Biology* **75**(Pt 2), 151–159.

Ebrahim A, Moreno-Chicano T, Appleby MV, Chaplin AK, Beale JH, Sherrell DA, Duyvesteyn HME, Owada S, Tono K, Sugimoto H, Strange RW, Worrall JAR, Axford D, Owen RL and Hough MA (2019*b*) Dose-resolved serial synchrotron and XFEL structures of radiation-sensitive metalloproteins. *IUCrJ* **6**(Pt 4), 543–551.

Emsley P, Lohkamp B, Scott WG and Cowtan K (2010) Features and development of Coot. *Acta Crystallographica. Section D, Biological Crystallography* **66**(Pt 4), 486–501.

Evans P (2006) Scaling and assessment of data quality. *Acta Crystallographica. Section D, Biological Crystallography* **62**(Pt 1), 72–82.

Feiler CG, Wallacher D and Weiss MS (2019) An all-in-one sample holder for macromolecular X-ray crystallography with minimal background scattering. *Journal of Visualized Experiments: JoVE* (149). DOI: 10.3791/59722.

Fenwick RB, Van Den Bedem H, Fraser JS and Wright PE (2014) Integrated description of protein dynamics from room-temperature X-ray crystallography and NMR. *Proceedings of the National Academy of Sciences of the United States of America* **111**, E445–E454.

Fink AL and Petsko GA (1981) X-ray cryoenzymology. *Advances in Enzymology and Related Areas of Molecular Biology* **52**, 177–246.

Fischer M, Coleman RG, Fraser JS and Shoichet BK (2014) Incorporation of protein flexibility and conformational energy penalties in docking screens to improve ligand discovery. *Nature Chemistry* **6**, 575–583.

Fischer M, Shoichet BK and Fraser JS (2015) One crystal, two temperatures: cryocooling penalties alter ligand binding to transient protein sites. *Chembiochem* **16**, 1560–1564.

Foadi J, Aller P, Alguel Y, Cameron A, Axford D, Owen RL, Armour W, Waterman DG, Iwata S and Evans G (2013) Clustering procedures for the optimal selection of data sets from multiple crystals in macromolecular crystallography. *Acta Crystallographica. Section D, Biological Crystallography* **69**(Pt 8), 1617–1632.

Förster A and Schulze-Briese C (2019) A shared vision for macromolecular crystallography over the next five years. *Structural Dynamics (Melville, N.Y.)* **6**, 064302.

Fraser JS, Clarkson MW, Degnan SC, Erion R, Kern D and Alber T (2009) Hidden alternative structures of proline isomerase essential for catalysis. *Nature* **462**, 669–673.

Fraser JS, Van Den Bedem H, Samelson AJ, Lang PT, Holton JM, Echols N and Alber T (2011) Accessing protein conformational ensembles using room-temperature X-ray crystallography. *Proceedings of the National Academy of Sciences of the United States of America* **108**, 16247–16252.

Frauenfelder H, Petsko GA and Tsernoglou D (1979) Temperature-dependent X-ray diffraction as a probe of protein structural dynamics. *Nature* **280**, 558–563.

Garman E (1999) Cool data: quantity AND quality. *Acta Crystallographica. Section D, Biological Crystallography* **55**(Pt 10), 1641–1653.

Garman EF (2010) Radiation damage in macromolecular crystallography: what is it and why should we care? *Acta Crystallographica. Section D, Biological Crystallography* **66**(Pt 4), 339–351.

Garman EF and Doublié S (2003) Cryocooling of macromolecular crystals: optimization methods. *Methods in Enzymology* **368**, 188–216.

Garman EF and Owen RL (2006) Cryocooling and radiation damage in macromolecular crystallography. *Acta Crystallographica. Section D, Biological Crystallography* **62**(Pt 1), 32–47.

Garman EF and Schneider TR (1997) Macromolecular cryocrystallography. *Journal of Applied Crystallography* **30**, 211–237.

Garman EF and Weik M (2017) Radiation damage in macromolecular crystallography. *Methods in Molecular Biology* **1607**, 467–489.

Gerlits O, Keen DA, Blakeley MP, Louis JM, Weber IT and Kovalevsky A (2017*a*) Room temperature neutron crystallography of drug resistant HIV-1 protease uncovers limitations of X-ray structural analysis at 100 K. *Journal of Medicinal Chemistry* **60**, 2018–2025.

https://doi.org/10.1017/S0033583520000128 Published online by Cambridge University Press

Gerlits OO, Coates L, Woods RJ and Kovalevsky A (2017*b*) Mannobiose binding induces changes in hydrogen bonding and protonation states of acidic residues in concanavalin A As revealed by neutron crystallography. *Biochemistry* **56**, 4747–4750.

Gerstel M, Deane CM and Garman EF (2015) Identifying and quantifying radiation damage at the atomic level. *Journal of Synchrotron Radiation* **22**, 201–212.

Giordano R, Leal RM, Bourenkov GP, McSweeney S and Popov AN (2012) The application of hierarchical cluster analysis to the selection of isomorphous crystals. *Acta Crystallographica. Section D, Biological Crystallography* **68**(Pt 6), 649–658.

Gotthard G, Aumonier S, De Sanctis D, Leonard G, Von Stetten D and Royant A (2019) Specific radiation damage is a lesser concern at room temperature. *IUCrJ* **6**(Pt 4), 665–680.

Grünbein ML and Nass Kovacs G (2019) Sample delivery for serial crystallography at free-electron lasers and synchrotrons. *Acta Crystallographica. Section D, Structural Biology* **75**(Pt 2), 178–191.

Haas DJ and Rossmann MG (1970) Crystallographic studies on lactate dehydrogenase at-75 degrees C. *Acta Crystallographica. Section B, Structural Science* **26**, 998–1004.

Halle B (2004) Biomolecular cryocrystallography: structural changes during flash-cooling. *Proceedings of the National Academy of Sciences of the United States of America* **101**, 4793–4798.

Hartmann H, Parak F, Steigemann W, Petsko GA, Ponzi DR and Frauenfelder H (1982) Conformational substates in a protein: structure and dynamics of metmyoglobin at 80 K. *Proceedings of the National Academy of Sciences of the United States of America* **79**, 4967–4971.

Hekstra DR, White KI, Socolich MA, Henning RW, Šrajer V and Ranganathan R (2016) Electric-field-stimulated protein mechanics. *Nature* **540**, 400–405.

Helliwell JR (2020) What is the structural chemistry of the living organism at its temperature and pressure? *Acta Crystallographica. Section D, Structural Biology* **76**(Pt 2), 87–93.

Henderson R (1990) Cryo-protection of protein crystals against radiation damage in electron and X-ray diffraction. *Proceedings of the Royal Society of London. Series B* **241**, 6–8.

Henzler-Wildman K and Kern D (2007) Dynamic personalities of proteins. *Nature* **450**, 964–972.

Holton JM (2009) A beginner's guide to radiation damage. *Journal of Synchrotron Radiation* **16**(Pt 2), 133–142.

Hope H (1988) Cryocrystallography of biological macromolecules: a generally applicable method. *Acta Crystallographica. Section B, Structural Science* **44**, 22–26.

Hope H, Frolow F, Von Böhlen K, Makowski I, Kratky C, Halfon Y, Danz H, Webster P, Bartels KS and Wittmann HG (1989) Cryocrystallography of ribosomal particles. *Acta Crystallographica. Section B, Structural Science* **45**(Pt 2), 190–199.

Huang GY, Gerlits OO, Blakeley MP, Sankaran B, Kovalevsky AY and Kim C (2014) Neutron diffraction reveals hydrogen bonds critical for cGMP-selective activation: insights for cGMP-dependent protein kinase agonist design. *Biochemistry* **53**, 6725–6727.

Jaeger K, Dworkowski F, Nogly P, Milne C, Wang M and Standfuss J (2016) Serial millisecond crystallography of membrane proteins. *Advances in Experimental Medicine and Biology* **922**, 137–149.

Juers DH and Matthews BW (2001) Reversible lattice repacking illustrates the temperature dependence of macromolecular interactions. *Journal of Molecular Biology* **311**, 851–862.

Juers DH and Matthews BW (2004) Cryo-cooling in macromolecular crystallography: advantages, disadvantages and optimization. *Quarterly Reviews of Biophysics* **37**, 105–119.

Juers DH, Farley CA, Saxby CP, Cotter RA, Cahn JKB, Holton-Burke RC, Harrison K and Wu Z (2018) The impact of cryosolution thermal contraction on proteins and protein crystals: volumes, conformation and order. *Acta Crystallographica. Section D, Structural Biology* **74**(Pt 9), 922–938.

Juette MF, Terry DS, Wasserman MR, Zhou Z, Altman RB, Zheng Q and Blanchard SC (2014) The bright future of single-molecule fluorescence imaging. *Current Opinion in Chemical Biology* **20**, 103–111.

Kalinin Y, Kmetko J, Bartnik A, Stewart A, Gillilan R, Lobkovsky E and Thorne R (2005) A new sample mounting technique for room-temperature macromolecular crystallography. *Journal of Applied Crystallography* **38**, 333–339.

Keedy DA (2019) Journey to the center of the protein: allostery from multitemperature multiconformer X-ray crystallography. *Acta Crystallographica. Section D, Structural Biology* **75**(Pt 2), 123–137.

Keedy DA, Van Den Bedem H, Sivak DA, Petsko GA, Ringe D, Wilson MA and Fraser JS (2014) Crystal cryocooling distorts conformational heterogeneity in a model Michaelis complex of DHFR. *Structure (London, England: 1993)* **22**, 899–910.

Keedy DA, Fraser JS and Van Den Bedem H (2015*a*) Exposing hidden alternative backbone conformations in X-ray crystallography using qFit. *PLoS Computational Biology* **11**, e1004507.

Keedy DA, Kenner LR, Warkentin M, Woldeyes RA, Hopkins JB, Thompson MC, Brewster AS, Van Benschoten AH, Baxter EL, Uervirojnangkoorn M, Mcphillips SE, Song J, Alonso-Mori R, Holton JM, Weis WI, Brunger AT, Soltis SM, Lemke H, Gonzalez A, Sauter NK, Cohen AE, Van Den Bedem H, Thorne RE and Fraser JS (2015*b*) Mapping the conformational landscape of a dynamic enzyme by multitemperature and XFEL crystallography. *Elife* **4**, e07574.

Keedy DA, Hill ZB, Biel JT, Kang E, Rettenmaier TJ, Brandão-Neto J, Pearce NM, Von Delft F, Wells JA and Fraser JS (2018) An expanded allosteric network in PTP1B by multitemperature crystallography, fragment screening, and covalent tethering. *Elife* **7**, e36307.

Kiefersauer R, Than ME, Dobbek H, Gremer L, Melero M, Strobl S, Dias JM, Soulimane T and Huber R (2000) A novel free-mounting system for protein crystals: transformation and improvement of diffraction power by accurately controlled humidity changes. *Journal of Applied Crystallography* **33**, 1223–1230.

King M (1954) An efficient method for mounting wet protein crystals for X-ray studies. *Acta Crystallographica* **7**, 601–602.

Kneller DW, Phillips G, Kovalevsky A and Coates L (2020*a*) Room-temperature neutron and X-ray data collection of 3CL M. *Acta Crystallographica. Section F, Structural Biology Communications* **76**(Pt 10), 483–487.

Kneller DW, Phillips G, O'neill HM, Jedrzejczak R, Stols L, Langan P, Joachimiak A, Coates L and Kovalevsky A (2020*b*) Structural plasticity of SARS-CoV-2 3CL M. *Nature Communications* **11**, 3202.

Kovácsová G, Grünbein ML, Kloos M, Barends TRM, Schlesinger R, Heberle J, Kabsch W, Shoeman RL, Doak RB and Schlichting I (2017) Viscous hydrophilic injection matrices for serial crystallography. *IUCrJ* **4** (Pt 4), 400–410.

Krojer T, Pike AC and Von Delft F (2013) Squeezing the most from every crystal: the fine details of data collection. *Acta Crystallographica. Section D, Biological Crystallography* **69**(Pt 7), 1303–1313.

Lang PT, Ng HL, Fraser JS, Corn JE, Echols N, Sales M, Holton JM and Alber T (2010) Automated electron-density sampling reveals widespread conformational polymorphism in proteins. *Protein Science* **19**, 1420–1431.

Leal RM, Bourenkov G, Russi S and Popov AN (2013) A survey of global radiation damage to 15 different protein crystal types at room temperature: a new decay model. *Journal of Synchrotron Radiation* **20**(Pt 1), 14–22.

Liebschner D, Rosenbaum G, Dauter M and Dauter Z (2015) Radiation decay of thaumatin crystals at three X-ray energies. *Acta Crystallographica. Section D, Biological Crystallography* **71**(Pt 4), 772–778.

Liebschner D, Afonine PV, Baker ML, Bunkóczi G, Chen VB, Croll TI, Hintze B, Hung LW, Jain S, Mccoy AJ, Moriarty NW, Oeffner RD, Poon BK, Prisant MG, Read RJ, Richardson JS, Richardson DC, Sammito MD, Sobolev OV, Stockwell DH, Terwilliger TC, Urzhumtsev AG, Videau LL, Williams CJ and Adams PD (2019) Macromolecular structure determination using X-rays, neutrons and electrons: recent developments in Phenix. *Acta Crystallographica. Section D, Structural Biology* **75**(Pt 10), 861–877.

Lieske J, Cerv M, Kreida S, Komadina D, Fischer J, Barthelmess M, Fischer P, Pakendorf T, Yefanov O, Mariani V, Seine T, Ross BH, Crosas E, Lorbeer O, Burkhardt A, Lane TJ, Guenther S, Bergtholdt J, Schoen S, Törnroth-Horsefield S, Chapman HN and Meents A (2019) On-chip crystallization for serial crystallography experiments and on-chip ligand-binding studies. *IUCrJ* **6**(Pt 4), 714–728.

https://doi.org/10.1017/S0033583520000128 Published online by Cambridge University Press

Low BW, Chen CC, Berger JE, Singman L and Pletcher JF (1966) Studies of insulin crystals at low temperatures: effects on mosaic character and radiation sensitivity. *Proceedings of the National Academy of Sciences of the United States of America* **56**, 1746–1750.

Lu S, Jang H, Gu S, Zhang J and Nussinov R (2016) Drugging Ras GTPase: a comprehensive mechanistic and signaling structural view. *Chemical Society Reviews* **45**, 4929–4952.

Makinen MW and Fink AL (1977) Reactivity and cryoenzymology of enzymes in the crystalline state. *Annual Review of Biophysics and Bioengineering* **6**, 301–343.

Maleknia SD, Brenowitz M and Chance MR (1999) Millisecond radiolytic modification of peptides by synchrotron X-rays identified by mass spectrometry. *Analytical Chemistry* **71**, 3965–3973.

Martiel I, Müller-Werkmeister HM and Cohen AE (2019) Strategies for sample delivery for femtosecond crystallography. *Acta Crystallographica. Section D, Structural Biology* **75**(Pt 2), 160–177.

Martin-Garcia JM, Conrad CE, Coe J, Roy-Chowdhury S and Fromme P (2016) Serial femtosecond crystallography: a revolution in structural biology. *Archives of Biochemistry and Biophysics* **602**, 32–47.

Martin-Garcia JM, Conrad CE, Nelson G, Stander N, Zatsepin NA, Zook J, Zhu L, Geiger J, Chun E, Kissick D, Hilgart MC, Ogata C, Ishchenko A, Nagaratnam N, Roy-Chowdhury S, Coe J, Subramanian G, Schaffer A, James D, Ketwala G, Venugopalan N, Xu S, Corcoran S, Ferguson D, Weierstall U, Spence JCH, Cherezov V, Fromme P, Fischetti RF and Liu W (2017) Serial millisecond crystallography of membrane and soluble protein microcrystals using synchrotron radiation. *IUCrJ* **4**(Pt 4), 439–454.

Martin-Garcia JM, Zhu L, Mendez D, Lee MY, Chun E, Li C, Hu H, Subramanian G, Kissick D, Ogata C, Henning R, Ishchenko A, Dobson Z, Zhang S, Weierstall U, Spence JCH, Fromme P, Zatsepin NA, Fischetti RF, Cherezov V and Liu W (2019) High-viscosity injector-based pink-beam serial crystallography of microcrystals at a synchrotron radiation source. *IUCrJ* **6**(Pt 3), 412–425.

Masson GR, Burke JE, Ahn NG, Anand GS, Borchers C, Brier S, Bou-Assaf GM, Engen JR, Englander SW, Faber J, Garlish R, Griffin PR, Gross ML, Guttman M, Hamuro Y, Heck AJR, Houde D, Iacob RE, Jørgensen TJD, Kaltashov IA, Klinman JP, Konermann L, Man P, Mayne L, Pascal BD, Reichmann D, Skehel M, Snijder J, Strutzenberg TS, Underbakke ES, Wagner C, Wales TE, Walters BT, Weis DD, Wilson DJ, Wintrode PL, Zhang Z, Zheng J, Schriemer DC and Rand KD (2019) Recommendations for performing, interpreting and reporting hydrogen deuterium exchange mass spectrometry (HDX-MS) experiments. *Nature Methods* **16**, 595–602.

Mathews II, Allison K, Robbins T, Lyubimov AY, Uervirojnangkoorn M, Brunger AT, Khosla C, Demirci H, Mcphillips SE, Hollenbeck M, Soltis M and Cohen AE (2017) The conformational flexibility of the acyltransferase from the disorazole polyketide synthase is revealed by an X-ray free-electron Laser using a room-temperature sample delivery method for serial crystallography. *Biochemistry* **56**, 4751–4756.

Meents A, Gutmann S, Wagner A and Schulze-Briese C (2010) Origin and temperature dependence of radiation damage in biological samples at cryogenic temperatures. *Proceedings of the National Academy of Sciences of the United States of America* **107**, 1094–1099.

Meents A, Wiedorn MO, Srajer V, Henning R, Sarrou I, Bergtholdt J, Barthelmess M, Reinke PYA, Dierksmeyer D, Tolstikova A, Schaible S, Messerschmidt M, Ogata CM, Kissick DJ, Taft MH, Manstein DJ, Lieske J, Oberthuer D, Fischetti RF and Chapman HN (2017) Pink-beam serial crystallography. *Nature Communications* **8**, 1281.

Mehrabi P, Schulz EC, Agthe M, Horrell S, Bourenkov G, Von Stetten D, Leimkohl JP, Schikora H, Schneider TR, Pearson AR, Tellkamp F and Miller RJD (2019*a*) Liquid application method for time-resolved analyses by serial synchrotron crystallography. *Nature Methods* **16**, 979–982.

Mehrabi P, Schulz EC, Dsouza R, Müller-Werkmeister HM, Tellkamp F, Miller RJD and Pai EF (2019*b*) Time-resolved crystallography reveals allosteric communication aligned with molecular breathing. *Science (New York, N.Y.)* **365**, 1167–1170.

Mehrabi P, Müller-Werkmeister HM, Leimkohl JP, Schikora H, Ninkovic J, Krivokuca S, Andriček L, Epp SW, Sherrell D, Owen RL, Pearson AR, Tellkamp F, Schulz EC and Miller RJD (2020) The HARE chip for efficient time-resolved serial synchrotron crystallography. *Journal of Synchrotron Radiation* **27**(Pt 2), 360–370.

Meisburger SP, Thomas WC, Watkins MB and Ando N (2017) X-ray scattering studies of protein structural dynamics. *Chemical Reviews* **117**, 7615–7672.

Mishin A, Gusach A, Luginina A, Marin E, Borshchevskiy V and Cherezov V (2019) An outlook on using serial femtosecond crystallography in drug discovery. *Expert Opinion on Drug Discovery* **14**, 933–945.

Mitchell EP and Garman EF (1994) Flash freezing of protein crystals: investigation of mosaic spread and diffraction limit with variation of cryoprotectant concentration. *Journal of Applied Crystallography* **27**, 1070–1074.

Moffat K (1989) Time-resolved macromolecular crystallography. *Annual Review of Biophysics and Biophysical Chemistry* **18**, 309–332.

Moffat K and Henderson R (1995) Freeze trapping of reaction intermediates. *Current Opinion in Structural Biology* **5**, 656–663.

Monteiro DCF, Vakili M, Harich J, Sztucki M, Meier SM, Horrell S, Josts I and Trebbin M (2019) A microfluidic flow-focusing device for low sample consumption serial synchrotron crystallography experiments in liquid flow. *Journal of Synchrotron Radiation* **26**(Pt 2), 406–412.

Monteiro DCF, Von Stetten D, Stohrer C, Sans M, Pearson AR, Santoni G, Van Der Linden P and Trebbin M (2020) 3D-MiXD: 3D-printed X-ray-compatible microfluidic devices for rapid, low-consumption serial synchrotron crystallography data collection in flow. *IUCrJ* **7**(Pt 2), 207–219.

Moreau DW, Atakisi H and Thorne RE (2019) Ice formation and solvent nanoconfinement in protein crystals. *IUCrJ* **6**(Pt 3), 346–356.

Mueller C, Marx A, Epp SW, Zhong Y, Kuo A, Balo AR, Soman J, Schotte F, Lemke HT, Owen RL, Pai EF, Pearson AR, Olson JS, Anfinrud PA, Ernst OP and Dwayne Miller RJ (2015) Fixed target matrix for femtosecond time-resolved and *in situ* serial micro-crystallography. *Structural Dynamics (Melville, N.Y.)* **2**, 054302.

Murakawa T, Baba S, Kawano Y, Hayashi H, Yano T, Kumasaka T, Yamamoto M, Tanizawa K and Okajima T (2019) Thermodynamic analysis of conformational change of the topaquinone cofactor in bacterial copper amine oxidase. *Proceedings of the National Academy of Sciences of the United States of America* **116**, 135–140.

Nave C and Garman EF (2005) Towards an understanding of radiation damage in cryocooled macromolecular crystals. *Journal of Synchrotron Radiation* **12**(Pt 3), 257–260.

Neutze R, Brändén G and Schertler GF (2015) Membrane protein structural biology using X-ray free electron lasers. *Current Opinion in Structural Biology* **33**, 115–125.

Nogly P, James D, Wang D, White TA, Zatsepin N, Shilova A, Nelson G, Liu H, Johansson L, Heymann M, Jaeger K, Metz M, Wickstrand C, Wu W, Båth P, Berntsen P, Oberthuer D, Panneels V, Cherezov V, Chapman H, Schertler G, Neutze R, Spence J, Moraes I, Burghammer M, Standfuss J and Weierstall U (2015) Lipidic cubic phase serial millisecond crystallography using synchrotron radiation. *IUCrJ* **2**(Pt 2), 168–176.

Oganesyan I, Lento C and Wilson DJ (2018) Contemporary hydrogen deuterium exchange mass spectrometry. *Methods (San Diego, Calif.)* **144**, 27–42.

Oghbaey S, Sarracini A, Ginn HM, Pare-Labrosse O, Kuo A, Marx A, Epp SW, Sherrell DA, Eger BT, Zhong Y, Loch R, Mariani V, Alonso-Mori R, Nelson S, Lemke HT, Owen RL, Pearson AR, Stuart DI, Ernst OP, Mueller-Werkmeister HM and Miller RJ (2016) Fixed target combined with spectral mapping: approaching 100% hit rates for serial crystallography. *Acta Crystallographica. Section D, Structural Biology* **72**(Pt 8), 944–955.

Owen RL, Rudiño-Piñera E and Garman EF (2006) Experimental determination of the radiation dose limit for cryocooled protein crystals. *Proceedings of the National Academy of Sciences of the United States of America* **103**, 4912–4917.

Owen RL, Paterson N, Axford D, Aishima J, Schulze-Briese C, Ren J, Fry EE, Stuart DI and Evans G (2014) Exploiting fast detectors to enter a new dimension in room-temperature crystallography. *Acta Crystallographica. Section D, Biological Crystallography* **70**(Pt 5), 1248–1256.

Owen RL, Axford D, Sherrell DA, Kuo A, Ernst OP, Schulz EC, Miller RJ and Mueller-Werkmeister HM (2017) Low-dose fixed-target serial synchrotron crystallography. *Acta Crystallographica. Section D, Structural Biology* **73**(Pt 4), 373–378.

Pawate AS, Šrajer V, Schieferstein J, Guha S, Henning R, Kosheleva I, Schmidt M, Ren Z, Kenis PJ and Perry SL (2015) Towards time-resolved

https://doi.org/10.1017/S0033583520000128 Published online by Cambridge University Press

serial crystallography in a microfluidic device. *Acta Crystallographica. Section F, Structural Biology Communications* **71**(Pt 7), 823–830.

Pearce NM, Krojer T and Von Delft F (2017) Proper modelling of ligand binding requires an ensemble of bound and unbound states. *Acta Crystallographica. Section D, Structural Biology* **73**(Pt 3), 256–266.

Petsko GA (1975) Protein crystallography at sub-zero temperatures: cryoprotective mother liquors for protein crystals. *Journal of Molecular Biology* **96**, 381–392.

Pflugrath JW (1999) The finer things in X-ray diffraction data collection. *Acta Crystallographica. Section D, Biological Crystallography* **55**(Pt 10), 1718–1725.

Pflugrath JW (2015) Practical macromolecular cryocrystallography. *Acta Crystallographica. Section F, Structural Biology Communications* **71**(Pt 6), 622–642.

Raich, L., Meier, K., Günther, J., Christ, C. D., Noé, F. and Olsson, S. (2020). Discovery of a hidden transient state in all bromodomain families. *bioRxiv*, 2020·2004·2001·019547.

Rajendran C, Dworkowski FS, Wang M and Schulze-Briese C (2011) Radiation damage in room-temperature data acquisition with the PILATUS 6M pixel detector. *Journal of Synchrotron Radiation* **18**(Pt 3), 318–328.

Ravelli RB and McSweeney SM (2000) The 'fingerprint' that X-rays can leave on structures. *Structure (London, England: 1993)* **8**, 315–328.

Riley BT, Wankowicz SA, De Oliveira SHP, Van Zundert GCP, Hogan D, Fraser JS, Keedy DA and Van Den Bedem H (2020) qFit 3: protein and ligand multiconformer modeling for X-ray crystallographic and single-particle cryo-EM density maps. *Protein Science*. DOI: 10.1002/pro.4001.

Ringe D and Petsko GA (2003) The 'glass transition' in protein dynamics: what it is, why it occurs, and how to exploit it. *Biophysical Chemistry* **105**, 667–680.

Roedig P, Duman R, Sanchez-Weatherby J, Vartiainen I, Burkhardt A, Warmer M, David C, Wagner A and Meents A (2016) Room-temperature macromolecular crystallography using a micro-patterned silicon chip with minimal background scattering. *Journal of Applied Crystallography* **49**(Pt 3), 968–975.

Roessler CG, Kuczewski A, Stearns R, Ellson R, Olechno J, Orville AM, Allaire M, Soares AS and Héroux A (2013) Acoustic methods for high-throughput protein crystal mounting at next-generation macromolecular crystallographic beamlines. *Journal of Synchrotron Radiation* **20**(Pt 5), 805–808.

Russi S, Juers DH, Sanchez-Weatherby J, Pellegrini E, Mossou E, Forsyth VT, Huet J, Gobbo A, Felisaz F, Moya R, McSweeney SM, Cusack S, Cipriani F and Bowler MW (2011) Inducing phase changes in crystals of macromolecules: status and perspectives for controlled crystal dehydration. *Journal of Structural Biology* **175**, 236–243.

Russi S, Gonzalez A, Kenner LR, Keedy DA, Fraser JS and Van Den Bedem H (2017) Conformational variation of proteins at room temperature is not dominated by radiation damage. *Journal of Synchrotron Radiation* **24**, 73–82.

Sanchez-Weatherby J, Bowler MW, Huet J, Gobbo A, Felisaz F, Lavault B, Moya R, Kadlec J, Ravelli RB and Cipriani F (2009) Improving diffraction by humidity control: a novel device compatible with X-ray beamlines. *Acta Crystallographica. Section D, Biological Crystallography* **65**(Pt 12), 1237–1246.

Santoni G, Zander U, Mueller-Dieckmann C, Leonard G and Popov A (2017) Hierarchical clustering for multiple-crystal macromolecular crystallography experiments: the. *Journal of Applied Crystallography* **50**(Pt 6), 1844–1851.

Scheidig AJ, Burmester C and Goody RS (1999) The pre-hydrolysis state of p21(ras) in complex with GTP: new insights into the role of water molecules in the GTP hydrolysis reaction of ras-like proteins. *Structure (London, England: 1993)* **7**, 1311–1324.

Schmidt M (2013) Mix and inject: reaction initiation by diffusion for time-resolved macromolecular crystallography. *Advances in Condensed Matter Physics* **2013**, 167276.

Schubert R, Kapis S, Gicquel Y, Bourenkov G, Schneider TR, Heymann M, Betzel C and Perbandt M (2016) A multicrystal diffraction data-collection approach for studying structural dynamics with millisecond temporal resolution. *IUCrJ* **3**(Pt 6), 393–401.

Schulz EC, Mehrabi P, Müller-Werkmeister HM, Tellkamp F, Jha A, Stuart W, Persch E, De Gasparo R, Diederich F, Pai EF and Miller RJD (2018) The hit-and-return system enables efficient time-resolved serial synchrotron crystallography. *Nature Methods* **15**, 901–904.

Skrzypczak-Jankun E, Bianchet MA, Mario Amzel L and Funk MO (1996) Flash-freezing causes a stress-induced modulation in a crystal structure of soybean lipoxygenase l3. *Acta Crystallographica. Section D, Biological Crystallography* **52**(Pt 5), 959–965.

Socher E and Sticht H (2016) Mimicking titration experiments with MD simulations: a protocol for the investigation of pH-dependent effects on proteins. *Scientific Reports* **6**, 22523.

Southworth-Davies RJ, Medina MA, Carmichael I and Garman EF (2007) Observation of decreased radiation damage at higher dose rates in room temperature protein crystallography. *Structure* **15**, 1531–1541.

Stellato F, Oberthür D, Liang M, Bean R, Gati C, Yefanov O, Barty A, Burkhardt A, Fischer P, Galli L, Kirian RA, Meyer J, Panneerselvam S, Yoon CH, Chervinskii F, Speller E, White TA, Betzel C, Meents A and Chapman HN (2014) Room-temperature macromolecular serial crystallography using synchrotron radiation. *IUCrJ* **1**(Pt 4), 204–212.

Teng T-Y (1990) Mounting of crystals for macromolecular crystallography in a free-standing thin film. *Journal of Applied Crystallography* **23**, 387–391.

Teng TY and Moffat K (2000) Primary radiation damage of protein crystals by an intense synchrotron X-ray beam. *Journal of Synchrotron Radiation* **7**(Pt 5), 313–317.

Thomaston JL, Woldeyes RA, Nakane T, Yamashita A, Tanaka T, Koiwai K, Brewster AS, Barad BA, Chen Y, Lemmin T, Uervirojnangkoorn M, Arima T, Kobayashi J, Masuda T, Suzuki M, Sugahara M, Sauter NK, Tanaka R, Nureki O, Tono K, Joti Y, Nango E, Iwata S, Yumoto F, Fraser JS and Degrado WF (2017) XFEL Structures of the influenza M2 proton channel: room temperature water networks and insights into proton conduction. *Proceedings of the National Academy of Sciences of the United States of America* **114**, 13357–13362.

Thompson MC, Cascio D and Yeates TO (2018) Microfocus diffraction from different regions of a protein crystal: structural variations and unit-cell polymorphism. *Acta Crystallographica. Section D, Structural Biology* **74**(Pt 5), 411–421.

Thorn A, Parkhurst J, Emsley P, Nicholls RA, Vollmar M, Evans G and Murshudov GN (2017) AUSPEX: a graphical tool for X-ray diffraction data analysis. *Acta Crystallographica. Section D, Structural Biology* **73**(Pt 9), 729–737.

Tilton RF, Dewan JC and Petsko GA (1992) Effects of temperature on protein structure and dynamics: X-ray crystallographic studies of the protein ribonuclease-A at nine different temperatures from 98 to 320 K. *Biochemistry* **31**, 2469–2481.

Tsujino S and Tomizaki T (2016) Ultrasonic acoustic levitation for fast frame rate X-ray protein crystallography at room temperature. *Scientific Reports* **6**, 25558.

Tyree TJ, Dan R and Thorne RE (2018) Density and electron density of aqueous cryoprotectant solutions at cryogenic temperatures for optimized cryoprotection and diffraction contrast. *Acta Crystallographica. Section D, Structural Biology* **74**(Pt 5), 471–479.

Van Den Bedem H and Fraser JS (2015) Integrative, dynamic structural biology at atomic resolution – it's about time. *Nature Methods* **12**, 307–318.

Van Den Bedem H, Dhanik A, Latombe JC and Deacon AM (2009) Modeling discrete heterogeneity in X-ray diffraction data by fitting multi-conformers. *Acta Crystallographica. Section D, Biological Crystallography* **65**(Pt 10), 1107–1117.

Van Den Bedem H, Bhabha G, Yang K, Wright PE and Fraser JS (2013) Automated identification of functional dynamic contact networks from X-ray crystallography. *Nature Methods* **10**, 896–902.

Van Zundert GCP, Hudson BM, De Oliveira SHP, Keedy DA, Fonseca R, Heliou A, Suresh P, Borrelli K, Day T, Fraser JS and Van Den Bedem H (2018) qFit-ligand reveals widespread conformational heterogeneity of drug-like molecules in X-ray electron density maps. *Journal of Medicinal Chemistry* **61**, 11183–11198.

Wall ME, Adams PD, Fraser JS and Sauter NK (2014) Diffuse X-ray scattering to model protein motions. *Structure (London, England: 1993)* **22**, 182–184.

Warkentin M and Thorne RE (2009) Slow cooling of protein crystals. *Journal of Applied Crystallography* **42**(Pt 5), 944–952.

Warkentin M and Thorne RE (2010) Glass transition in thaumatin crystals revealed through temperature-dependent radiation-sensitivity measurements. *Acta Crystallographica. Section D, Biological Crystallography* **66**(Pt 10), 1092–1100.

Warkentin M, Badeau R, Hopkins J and Thorne RE (2011) Dark progression reveals slow timescales for radiation damage between T = 180 and 240 K. *Acta Crystallographica. Section D, Biological Crystallography* **67**(Pt 9), 792–803.

Warkentin M, Hopkins JB, Badeau R, Mulichak AM, Keefe LJ and Thorne RE (2013) Global radiation damage: temperature dependence, time dependence and how to outrun it. *Journal of Synchrotron Radiation* **20**(Pt 1), 7–13.

Watt W, Tulinsky A, Swenson RP and Watenpaugh KD (1991) Comparison of the crystal structures of a flavodoxin in its three oxidation states at cryogenic temperatures. *Journal of Molecular Biology* **218**, 195–208.

Weik M and Colletier JP (2010) Temperature-dependent macromolecular X-ray crystallography. *Acta Crystallographica. Section D, Biological Crystallography* **66**(Pt 4), 437–446.

Weik M, Vernede X, Royant A and Bourgeois D (2004) Temperature derivative fluorescence spectroscopy as a tool to study dynamical changes in protein crystals. *Biophysical Journal* **86**, 3176–3185.

Weinert T, Olieric N, Cheng R, Brünle S, James D, Ozerov D, Gashi D, Vera L, Marsh M, Jaeger K, Dworkowski F, Panepucci E, Basu S, Skopintsev P, Doré AS, Geng T, Cooke RM, Liang M, Prota AE, Panneels V, Nogly P, Ermler U, Schertler G, Hennig M, Steinmetz MO, Wang M and Standfuss J (2017) Serial millisecond crystallography for routine room-temperature structure determination at synchrotrons. *Nature Communications* **8**, 542.

Wickstrand C, Nogly P, Nango E, Iwata S, Standfuss J and Neutze R (2019) Bacteriorhodopsin: structural insights revealed using X-ray lasers and synchrotron radiation. *Annual Review of Biochemistry* **88**, 59–83.

Wierman JL, Paré-Labrosse O, Sarracini A, Besaw JE, Cook MJ, Oghbaey S, Daoud H, Mehrabi P, Kriksunov I, Kuo A, Schuller DJ, Smith S, Ernst OP, Szebenyi DME, Gruner SM, Miller RJD and Finke AD (2019) Fixed-target serial oscillation crystallography at room temperature. *IUCrJ* **6**(Pt 2), 305–316.

Winter G, Waterman DG, Parkhurst JM, Brewster AS, Gildea RJ, Gerstel M, Fuentes-Montero L, Vollmar M, Michels-Clark T, Young ID, Sauter NK and Evans G (2018) DIALS: implementation and evaluation of a new integration package. *Acta Crystallographica. Section D, Structural Biology* **74**(Pt 2), 85–97.

Wlodawer A, Minor W, Dauter Z and Jaskolski M (2008) Protein crystallography for non-crystallographers, or how to get the best (but not more) from published macromolecular structures. *FEBS Journal* **275**, 1–21.

Wolff AM, Young ID, Sierra RG, Brewster AS, Martynowycz MW, Nango E, Sugahara M, Nakane T, Ito K, Aquila A, Bhowmick A, Biel JT, Carbajo S, Cohen AE, Cortez S, Gonzalez A, Hino T, Im D, Koralek JD, Kubo M, Lazarou TS, Nomura T, Owada S, Samelson AJ, Tanaka T, Tanaka R, Thompson EM, Van Den Bedem H, Woldeyes RA, Yumoto F, Zhao W, Tono K, Boutet S, Iwata S, Gonen T, Sauter NK, Fraser JS and Thompson MC (2020) Comparing serial X-ray crystallography and microcrystal electron diffraction (MicroED) as methods for routine structure determination from small macromolecular crystals. *IUCrJ* **7**(Pt 2), 306–323.

Zeldin OB, Brockhauser S, Bremridge J, Holton JM and Garman EF (2013*a*) Predicting the X-ray lifetime of protein crystals. *Proceedings of the National Academy of Sciences of the United States of America* **110**, 20551–20556.

Zeldin OB, Gerstel M and Garman EF (2013*b*) Optimizing the spatial distribution of dose in X-ray macromolecular crystallography. *Journal of Synchrotron Radiation* **20**(Pt 1), 49–57.

Zhao FZ, Zhang B, Yan EK, Sun B, Wang ZJ, He JH and Yin DC (2019) A guide to sample delivery systems for serial crystallography. *FEBS Journal* **286**, 4402–4417.

https://doi.org/10.1017/S0033583520000128 Published online by Cambridge University Press